# **The Multiple Facets of Correlation Functions**

The notion of correlation function, defined in Chapter 10, can be extended and adapted toward the study of a wide range of observables designed to investigate specific aspects of nuclear collision dynamics or properties of the matter produced in elementary particle and nuclear collisions. Figure 11.1 displays an overview of the many correlation functions and fluctuation measures commonly used by particle and nuclear physics in their study of nuclear collisions.

In this chapter, we examine several types of correlation functions in detail, beginning with a discussion of two-particle differential correlation functions in §11.1 and a cursory look at three-particle correlations in §11.2. Several integral correlators commonly used in high-energy nuclear for measurements of event-by-event fluctuations are presented in §11.3. The chapter ends with a comprehensive discussion of flow measurement techniques.

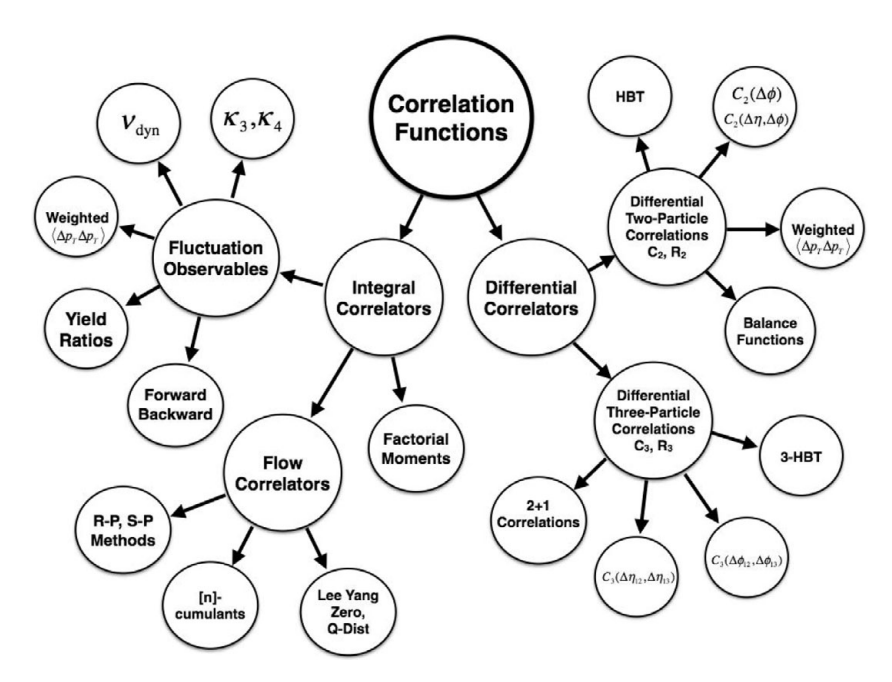
### 11.1 Two-Particle Correlation Functions

Two-particle correlation functions play an important role in the study of collision dynamics in nucleus-nucleus collisions as well as in elementary particle interactions (e.g., pp,  $\bar{p}p$ ,  $e^+e^-$ , ep, and so on). Azimuthal correlations, in particular, have been instrumental in the discovery of jet quenching by the opaque and dense medium (QGP) formed in central A–A collisions studied at the Relativistic Heavy-Ion Collider (BNL) and the Large Hadron Collider (CERN) [11]. Such correlations may be studied between indistinguishable particles in identical kinematic ranges, or with particles of different types, species, or belonging to distinct kinematic ranges.

We begin with a description of two-particle azimuthal correlations in §11.1.1 and extend the discussion to joint azimuthal and rapidity correlations in §11.1.2.

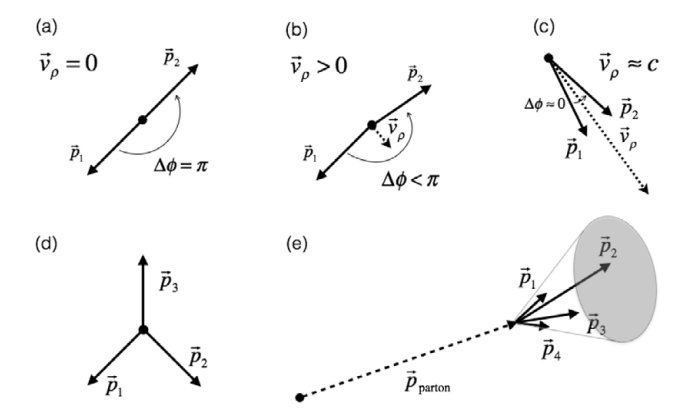
#### 11.1.1 Two-Particle Azimuthal Correlation Functions

Momentum and energy conservation impart a specific relation between particles produced by elementary processes. For instance, a  $\rho^0$ -meson decaying at rest in the laboratory is expected to produce a pair of  $\pi^+$  and  $\pi^-$  that fly back-to-back in this frame of reference. This means the two pions should be emitted with an angle of  $180^\circ$  relative to one another, as illustrated in Figure 11.2a. However, if the  $\rho$ -meson is in slow motion, the pions will not be seen exactly back-to-back but with a slightly smaller angle than  $180^\circ$ . And if the  $\rho^0$  travels at high velocity in the lab frame, the pions will appear to be focused in nearly the same



The multiple facets of correlation functions. Differential and integral correlations have a common basis in terms of cumulants, and enable the definition of several types of correlation observables, many of which are shown in this figure and discussed in this chapter.

direction and will thus be observed with a very small relative angle. Two-particle decays of other resonances produce qualitatively similar results. Three-particle decays at rest might produce Mercedes topologies, termed this because of their similarity to the Mercedes-Benz logo, as shown in Figure 11.2d, while parton fragmentation yields collimated particle production in the forms of jets consisting of several particles emitted in relatively narrow cone,



Momentum vectors of  $\pi$ -mesons produced by  $\rho$ -meson decays (a) at rest, (b) at small velocity, and (c) at very large velocity (near speed of light). (d) 3-prong resonance decay at rest. (e) Jet: emission of several hadrons in a narrow cone surrounding the direction of a fragmenting parton.

Fig. 11.2

as illustrated in Figure 11.2e. Of course, a typical elementary collision might involve a random selection or/and superposition of several of these and other processes. Two-particle distributions in relative angle may thus become arbitrarily complex. Still, understanding the specific mechanisms that lead to particle production may be possible if one can identify specific correlation features. This said, since the number of particles produced in elementary processes (and even more so in nucleus—nucleus collisions) can be rather large, and given that not all particle pairs may be correlated (i.e., result from a common process), it is useful to consider the use of two-particle cumulants to identify the strength of two particle correlations. Recall from §10.2 that while two-particle densities  $\rho_2(y_1, y_2)$  are sensitive to the number of particle pairs produced, they do not readily provide an unambiguous indication of the degree of correlation of these pairs. Different reaction mechanisms may lead to different correlation topologies (e.g., in terms of relative azimuthal angle), and thus it is indeed necessary to use cumulants to properly gauge the degree of correlation between measured pairs.

#### **Observable Definition: Two-Particle Cumulant**

We begin our discussion for pairs of "identical" particles measured in the same kinematic range. In §10.2, we defined generic two-particle cumulant  $C_2$  in terms of kinematic variables  $y_1$  and  $y_2$  as

$$C_2(y_1, y_2) = \rho_2(y_1, y_2) - \rho_1(y_1)\rho_1(y_2), \tag{11.1}$$

where  $\rho_1(y_i)$  and  $\rho_2(y_1, y_2)$  represent single and pair densities expressed as function of kinematical variables  $y_1$  and  $y_2$ , respectively. We also introduced normalized cumulants  $R_2$ ,

$$R_2(y_1, y_2) = \frac{\rho_2(y_1, y_2)}{\rho_1(y_1)\rho_1(y_2)} - 1,$$
(11.2)

which effectively carry the same information about the correlations between produced particles. We here restrict the two variables  $y_1$  and  $y_2$  to specifically represent the azimuthal production angles  $\phi_1$  and  $\phi_2$  of the two particles of interest, and write

$$C_2(\phi_1, \phi_2) = \rho_2(\phi_1, \phi_2) - \rho_1(\phi_1)\rho_1(\phi_2)$$
(11.3)

$$R_2(\phi_1, \phi_2) = \frac{\rho_2(\phi_1, \phi_2)}{\rho_1(\phi_1)\rho_1(\phi_2)} - 1,$$
(11.4)

where the densities  $\rho_1(\phi_i)$  and  $\rho_2(\phi_1, \phi_2)$  are measured/calculated for specific ranges  $p_{T, \min} \leq p_T < p_{T, \max}$  and  $\eta_{T, \min} \leq \eta_T < \eta_{T, \max}$ . From a theoretical standpoint, in the absence of polarization or other discriminating direction or axis, one expects the single particle yield should have no dependence on  $\phi$ ,

$$\rho_1(\phi_1) = \rho_1(\phi_2) \equiv \bar{\rho}_1,$$
(11.5)

while the strength of the correlation function  $C_2$  should depend only on the relative angle  $\Delta \phi = \phi_1 - \phi_2$ . It is thus of interest to recast the correlation function in terms of  $\Delta \phi$  exclusively. Toward that end, consider the change of variable

$$\phi_1, \phi_2 \rightarrow \Delta \phi = \phi_1 - \phi_2, \quad \bar{\phi} = (\phi_1 + \phi_2)/2$$
 (11.6)

with the Jacobian  $J = \left| \partial \left( \Delta \phi, \bar{\phi} \right) / \partial \left( \phi_1, \phi_2 \right) \right| = 1$ . This yields a correlation function  $C_2$  that can in principle depend on both  $\Delta \phi$  and  $\bar{\phi}$ . But given the collision system is not polarized and the reaction plane of the colliding particles (nuclei) is not explicitly determined, particle production must be invariant under rotation in  $\bar{\phi}$ . It is thus legitimate to average out (marginalize) this coordinate. One consequently gets a correlation function  $C_2$  that depends exclusively on the relative angle  $\Delta \phi$  of the particles:

$$C_2(\Delta\phi) = \rho_2(\Delta\phi) - \frac{1}{2\pi} \int_0^{2\pi} \bar{\rho}_1^2 d\bar{\phi},$$

$$= \rho_2(\Delta\phi) - \bar{\rho}_1^2,$$
(11.7)

where, in the second line, we used the fact that  $\rho_1^2$  is a constant and can be taken out of the integral. Given  $R_2$  is a ratio, one can consider two distinct approaches to average out the  $\bar{\phi}$  coordinate. The first involves a ratio of averages while the second consists of the average of a ratio. In general, one can in fact use two approaches for the determination of  $C_2$  and  $C_2$ . Indeed, one can first proceed to estimate these correlation functions in terms of both  $C_2$  and  $C_3$  with a subsequent average over  $\bar{\phi}$  to obtain functions of  $C_3$  only. Alternatively, one can seek estimates of either function directly in terms of  $C_3$  approach is more common and is therefore referred as **Method 1** ( $C_3$ ) in the following:

### Method 1 (M1)

$$C_2^{(M1)}(\Delta\phi) = \rho_2(\Delta\phi) - \rho_1 \otimes \rho_1(\Delta\phi) \tag{11.8}$$

$$R_2^{(M1)}(\Delta\phi) = \frac{\rho_2(\Delta\phi)}{\rho_1 \otimes \rho_1(\Delta\phi)} - 1, \tag{11.9}$$

where the term  $\rho_1 \otimes \rho_1(\Delta \phi)$  may be evaluated either through an event-mixing technique or by averaging the product  $\rho_1(\phi_1)\rho_1(\phi_2)$  over  $\bar{\phi}$ .

**Method 2** (M2) first requires the determination of both the single and pair densities in terms of  $\phi_1$  and  $\phi_2$  explicitly. The two functions are subsequently obtained as averages over  $\bar{\phi}$ :

#### Method 2 (M2)

$$C_2^{(M2)}(\Delta\phi) = \iiint_0^{2\pi} \left\{ \rho_2(\phi_1, \phi_2) - \rho_1(\phi_1)\rho_1(\phi_2) \right\}$$
 (11.10)

$$\times \, \delta(\Delta\phi - \phi_1 + \phi_2) \delta(\bar{\phi} - (\phi_1 + \phi_2)/2) \, d\phi_1 d\phi_2 d\bar{\phi}$$

$$R_2^{(M2)}(\Delta\phi) = \iiint_0^{2\pi} R_2(\phi_1, \phi_2)$$

$$\times \delta(\Delta\phi - \phi_1 + \phi_2)\delta(\bar{\phi} - (\phi_1 + \phi_2)/2) d\phi_1 d\phi_2 d\bar{\phi}.$$
(11.11)

where

$$R_2(\phi_1, \phi_2) = \frac{C_2(\phi_1, \phi_2)}{\rho_1(\phi_1)\rho_1(\phi_2)}$$

$$= \frac{\rho_2(\phi_1, \phi_2)}{\rho_1(\phi_1)\rho_1(\phi_2)} - 1$$
(11.12)

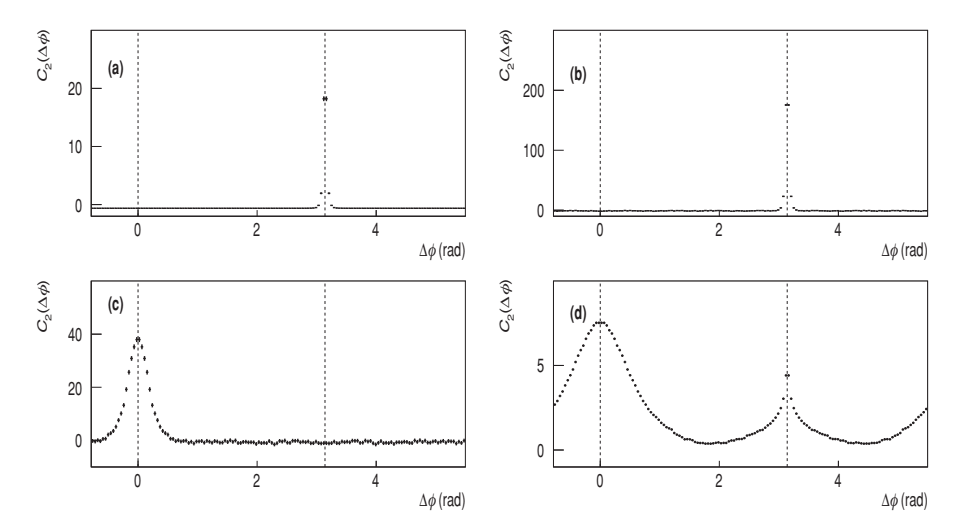


Fig. 11.3 Correlation function  $C_2$  of  $\rho^0$ -meson decaying (a, b) near rest, (c) at very large velocity in the laboratory reference frame, and (d) over a "realistic" range of velocities spanning values from zero up to nearly the speed of light. In (a), the number of  $\rho^0$  was fixed to one per event, while in (b-d), it is set to fluctuate randomly from five to ten  $\rho^0$  per event. Distributions have been "shifted" in  $\Delta \phi$  for purely esthetic reasons. Dashed lines are drawn at  $\Delta \phi = 0$  and  $\Delta \phi = 0$  to quide the eye.

For angles  $\phi_1$  and  $\phi_2$  in the range  $[0, 2\pi]$ , one obtains a difference  $\Delta \phi = \phi_1 - \phi_2$  in the range  $[-2\pi, 2\pi]$ . However, by virtue of the system's symmetry, this range may be reduced to  $[0, \pi]$  and other components of the  $[-2\pi, 2\pi]$  range are redundant and usually shifted onto  $[0, \pi]$ . It should thus be understood that the preceding integrals over  $\phi_1$  and  $\phi_2$  are evaluated onto  $0 \le \Delta \phi \le \pi$ , and often symmetrized about  $\pi$  and plotted in the range  $[0, 2\pi]$ , or shifted and plotted in  $[-\pi, 3\pi/2]$  for ease of visualization. From a theoretical standpoint, it is easy to show that the two methods yield identical results for  $\Delta \phi$  correlations, since the single particle yield is invariant under azimuthal rotation, that is,  $\rho_1(\phi_1) = \rho_1(\phi_2) \equiv \bar{\rho}_1$ . We will see in §12.4, where we discuss methods to account for instrumental effects, that both M1 and M2 yield robust measurements of  $R_2(\Delta \phi)$ . Measurements of  $C_2$ , however, require efficiency corrections in either method. Additionally, while M2 may be subject to aliasing because of the finite size of the bins used to obtain estimates of the densities  $\rho_1$  and  $\rho_2$ , we will also show in §12.4 that M1 is not strictly robust when measurements are extended to involve dependencies on other coordinates such as the rapidity of the particles, or their differences.

# **Example 1: Resonance Decays**

A great variety of dynamical processes such as jet production, resonance decays, and collective flow can shape azimuthal correlation functions. Figure 11.3 presents examples of correlation functions,  $C_2(\Delta \phi)$ , obtained with Monte Carlo simulations of collisions

<sup>&</sup>lt;sup>1</sup> Unaffected by instrumental effects, most particularly detection efficiencies.

producing charged pion pairs  $(\pi^+ + \pi^-)$  by decays of  $\rho^0$ -mesons. Figure 11.3a displays the correlation function of events involving a single  $\rho^0$  decaying near rest in the lab frame yield. One observes a prominent away-side peak centered at  $\Delta \phi = \pi$ , which corresponds to pion pairs being emitted essentially back-to-back. Emission from  $\rho^0$  at rest would produce a narrow peak at  $\Delta \phi = \pi$  exactly, but moving  $\rho^0$ s produce pairs that are not strictly back-to-back and consequently lead to a finite width peak centered at  $\Delta \phi = \pi$ . Also note that because the number of  $\rho^0$  is fixed, so is the number of pions because no efficiency losses or acceptance cuts were accounted for in the generation of this plot. A fixed number of particles effectively produces a multinomial behavior. The total multiplicity is fixed, and the pions can fall in a wide variety of bins. The covariance of the yields for  $\Delta \phi$  values outside the peak thus tend to be negative. This effect disappears if the  $\rho^0$  multiplicity fluctuates, as illustrated in Figure 11.3b, which was computed with a uniformly distributed random number of  $\rho^0$  in the range 5–10. However, as illustrated in Figure 11.3c, the correlation peak shifts to the origin (i.e.,  $\Delta \phi = 0$ ) if the  $\rho^0$ -decays take place at very large momentum in the lab frame. In practice, resonances such as the  $\rho^0$  are produced over a large range of momenta, one then observes a more complicated correlation function, as shown in Figure 11.3d, which combines peaks at both the origin and at  $\Delta \phi = \pi$ .

### **Example 2: Correlations from Anisotropic Flow**

Two-particle correlations are also very much influenced by collective effects. For instance, collisions of heavy nuclei at finite impact parameter, illustrated in Figure 11.4, may lead to the production of a very dense but inhomogeneous and anisotropic medium or system. The expansion of this medium, through pressure or momentum transfer gradients, is understood to lead to collective motion and anisotropic emission of low to medium  $p_T$  particles in the plane transverse to the beam axis. High-energy partons produced within this medium are also believed to be subject to differential energy loss according to the pathlength they traverse to exit the medium, thereby leading to complementary high  $p_T$  anisotropic emission patterns. Both effects are commonly known as **anisotropic flow**. While general techniques to measure flow are discussed in §11.4, we demonstrate, in the remainder of this section, that collective particle motion may readily be identified with simple two-particle cumulants  $C_2(\Delta \phi)$  and/or normalized cumulants  $R_2(\Delta \phi)$ .

On general grounds, let us assume that nucleus–nucleus collisions produce, on an event-by-event basis, systems that are inhomogeneous and anisotropic, as illustrated in Figure 11.4a. One can model the system (energy density) spatial anisotropy in terms of a simple Fourier decomposition relative to the origin O:

$$\rho(\phi, r) = f(r) \left( 1 + \sum_{n=1}^{\infty} \epsilon_n \cos(n\phi) \right). \tag{11.13}$$

The dynamics of the collisions leads to system expansion and particle emission that reflect the magnitude of the spatial anisotropy coefficients  $\epsilon_n$ . One can then model the collective motion of particles produced by the system as a Fourier expansion in momentum space,

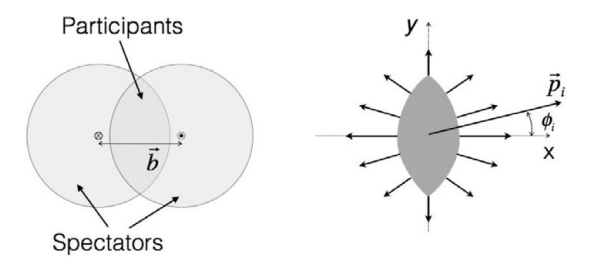


Fig. 11.4

Schematic illustration of the transverse profile of the participant matter produced in high-energy heavy-ion collisions. The participant region features pressure gradients which propel particle outward anisotropically in the transverse plane.

relative to the collision impact parameter vector,  $\vec{b}$ :

$$\rho(\phi_i|\psi) = \bar{\rho} \left\{ 1 + 2 \sum_{n=1}^{\infty} v_n \cos(n(\phi_i - \psi)) \right\},$$
(11.14)

where  $\bar{\rho}$  is the average particle density,  $\phi$  is the angle of emission of the particles, and  $\psi$  is the orientation angle of the reaction plane in the laboratory frame of reference. Since the impact parameter is not readily observed, one must average over all possible orientations of the reaction plane to get the observed single particle density:

$$\rho_1(\phi_i) = \int_0^{2\pi} d\psi \, \rho_1(\phi_i|\psi) P(\psi) = \bar{\rho}. \tag{11.15}$$

The orientation of the reaction plane,  $\psi$ , is assumed to vary collision by collision uniformly in the range  $[0, 2\pi]$  and is given a probability  $P(\psi) = (2\pi)^{-1}$ . The integration in (11.15) thus indeed yields  $\bar{\rho}$ , the average particle density. The density of particle pairs has a less trivial behavior, however. At fixed  $\psi$ , we model the two-particle density as

$$\rho_2(\phi_1, \phi_2 | \psi) = \bar{\rho}^2 \left\{ 1 + 2 \sum_{n=1}^{\infty} v_n \cos(n(\phi_1 - \psi)) \right\}$$

$$\times \left\{ 1 + 2 \sum_{n=1}^{\infty} v_n \cos(n(\phi_2 - \psi)) \right\}.$$
(11.16)

Given  $\psi$  is not explicitly measured, the two-particle density must be averaged over all equally probable values of this angle. One finds

$$\rho_2(\phi_1, \phi_2) = (2\pi)^{-1} \int_0^{2\pi} \rho_2(\phi_1, \phi_2 | \psi) d\psi$$

$$= \bar{\rho}^2 \left\{ 1 + 2 \sum_{n=1}^{\infty} (v_n)^2 \cos(n(\phi_1 - \phi_2)) \right\}$$
(11.17)

and concludes that the spatial anisotropy of the collisions may lead to observable anisotropies in momentum space. The harmonic coefficients  $v_n$  are commonly known as **flow coefficients**. Their magnitudes have been measured in a variety of collision systems

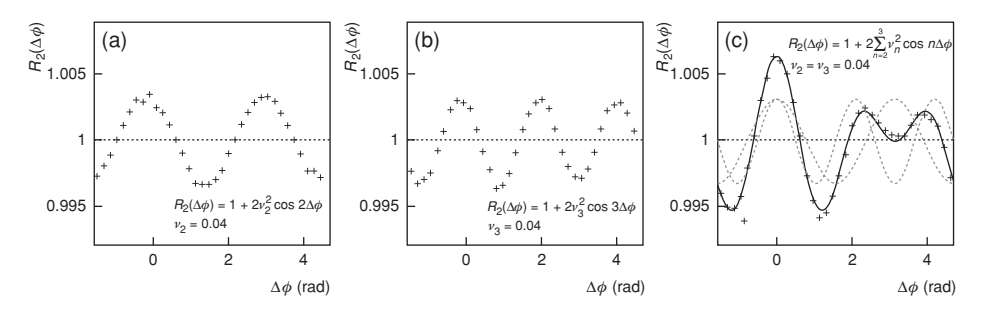


Fig. 11.5

Simulations of  $R_2(\Delta\phi)$  correlation functions determined by anisotropic flow. (a) Simulated elliptic flow with  $v_2=0.04$ . (b) Simulated triangular flow with  $v_3=0.04$ , (c) combination of elliptic and triangular flow with  $v_2=v_3=0.04$ , which produces an away-side dip at  $\Delta\phi=\pi$  similar to those observed in central Heavy-lon collisions by several RHIC and LHC experiments [1]. The dashed and solid lines display the Fourier components used in the simulation and their sum, respectively.

at several beam energies. In high-energy nucleus-nucleus the  $v_2$  coefficients are typically the largest. The  $v_3$  are also found to be significant, even in symmetric collision systems (e.g., Au–Au, or Pb–Pb), most likely the result of fluctuations in the initial spatial configurations of the colliding nuclei. Higher-order coefficients,  $v_{n\geq 4}$ , are typically much smaller than either  $v_2$  or  $v_3$  coefficients [182].

Figure 11.5 displays simulated  $R_2(\Delta \phi)$  correlation functions obtained for selected values of flow coefficients  $v_2$  and  $v_3$ . Note how the particular combination of coefficients  $v_2 = v_3 = 0.04$ , shown in panel (c), produces an away-side "dip" featured in many observed distributions measured in central A-A collisions at RHIC and LHC energies [1].

# **Semi-inclusive and Species Dependent Correlation Functions**

As we saw earlier, resonance production and flow lead to varied correlation shapes in azimuth. To further complicate the interpretation of correlation functions, consider that jet fragmentation and other particle production processes such as "string fragmentation" have their own signatures also in two-particle azimuthal correlations. The fragmentation of a single jet in particular produces a strong and broad peak centered at  $\Delta \phi = 0$ , while the production of di-jets features both a near-side peak ( $\Delta \phi = 0$ ) and an away-side peak  $(\Delta \phi = \pi)$ . The strength, shape, and width of these peaks are known to depend on the jet transverse momentum and particle multiplicity (number of particles composing the jet). All in all, the structure of correlation functions measured in p-p collisions are typically the result of a random superposition of several production processes that depend on the collision energy, as well as the number and species of particles produced. Correlation functions produced in heavy-ion collisions are further "enriched" by collective processes, such as the anisotropic flow discussed earlier, and radial (or outward) flow effects discussed in [181]. Inclusive measurements of two-particle azimuthal correlation functions are consequently insufficient, typically, to fully pinpoint the collision dynamics. Researchers have thus sought to study more exclusive correlation functions (e.g., azimuthal correlation as a function of particle multiplicity), for specific particle species or by adding additional kinematic constraints. One may also gain further insight into the nature of the particle production processes by studying correlations as a function of the particle momenta and rapidity (pseudorapidity).

Correlation functions of distinguishable particle types or species are readily defined on the basis of Eq. (11.3), and both M1 and M2 may be used to carry out measurements of these functions. The correlation measurements discussed earlier in this section can thus be straightforwardly extended to correlation studies of particles of different charge or species (e.g.,  $\pi^+$  vs.  $\pi^-$ , or  $\pi$  vs. K, and so on), or for particles in different momentum (or rapidity) ranges, discussed in the next subsection.

# Triggered Correlation Functions

Correlation functions involving one high- and one low- $p_T$  particle are particularly useful to study and characterize the production of jets in both p-p and A-A collisions without actually resorting to a full-fledged jet-finding analysis. Correlation studies of this type are commonly known as triggered correlation functions, even though no actual trigger is actually involved in such studies. Triggered correlation functions have been instrumental in unravelling the existence of jet quenching in Au-Au collisions at RHIC [11].

The study of triggered correlation functions typically requires the trigger particle to be at much higher  $p_T$  than the second particle, known as the associate. The production of the trigger particle may consequently be **rare**. It is thus legitimate to count the number of associates found in a given event, relative to the trigger particle. Labeling the trigger particle as T and the associates as A, one may define a triggered correlation as

$$C_{T,A}(\Delta\phi) = \frac{\rho_2(\Delta\phi)}{\langle N_T \rangle},\tag{11.18}$$

where

$$\rho_2(\Delta\phi) = \int_{\Omega_T} \int_{\Omega_A} \rho_2(\eta_T, \phi_T, p_{\perp,T}, \eta_A, \phi_A, p_{\perp,A})$$
(11.19)

$$imes \delta(\Delta\phi - \phi_T + \phi_A) d\eta_T d\phi_T dp_{\perp,T} d\eta_A d\phi_A dp_{\perp,A}$$

$$\langle N_T \rangle = \int_{\Omega} \rho_T(\eta_T, \phi_T, p_{\perp, T}) \, d\eta_T, d\phi_T, dp_{\perp, T}, \tag{11.20}$$

The integration is taken over the volumes  $\Omega_i$ , i=T, A, that specify the kinematic range in which the trigger and associates are measured. The numerator  $\rho_2(\Delta\eta)$  corresponds to the average number of trigger–associate pairs detected as a function of the relative azimuthal angle  $\Delta\phi$ , while the denominator  $\langle N_T \rangle$  corresponds to the average number of trigger particles altogether detected, in a given dataset, or under some specific event selection criteria. Effectively,  $C_{T,A}(\Delta\phi)$  provides the average number of associates, vs.  $\Delta\phi$ , per trigger particle. A measurement of  $C_{T,A}(\Delta\phi)$  may be implemented by taking the ratio of the average number of trigger–associate pairs per event by the average number of trigger particles

per event:

$$C_{T,A}(\Delta \phi) = \frac{\sum_{\alpha=1}^{N'_{ev}} N_{T,A}(\Delta \eta)}{\sum_{\alpha=1}^{N'_{ev}} N_{T,\alpha}}$$
(11.21)

where the sums are computed only for events containing a trigger particle. Triggered correlations are typically of greatest interest for jet-like trigger particles. Those have a low production cross section and only a small fraction of the events are thus expected to contain a trigger particle. If there is at most one trigger particle per event, one may write

$$C_{T,A}(\Delta \phi) = \frac{1}{N'_{ev}} \sum_{\alpha=1}^{N'_{ev}} N_{T,A}(\Delta \eta)$$
 (11.22)

where the sum is taken over events containing one trigger particle. For kinematical conditions such that there is typically more than one trigger particle per event, there is a common practice that consists in defining  $C_{T,A}(\Delta \phi)$  as

$$C_{T,A}^{\text{ebye}}(\Delta\phi) = \frac{1}{N_{ev}'} \sum_{\alpha=1}^{N_{ev}'} \frac{N_{T,A}(\Delta\eta)}{N_T}$$
 (11.23)

where  $N_T$  stands for the number of trigger particle measured in each event (the sum being carried out only on events with at least one trigger particle). In general, this formulation is expected to yield values in qualitative agreement to those obtained with Eq. (11.21). Quantitative difference of several percent may, however, occur. And while this latter formulation of the correlation function may seem more natural, it does not lend itself to a simple definition in terms of single- and two-particle densities such as Eq. (11.21). The inclusive formulation, though seemingly less intuitive, is thus usually preferred.

It is also important to realize that  $C_{T,A}(\Delta \phi)$  is not a correlation function in the strict sense of the word, since it does not involve subtraction of purely combinatorial contributions. This is not a serious problem, however, as long as the trigger particle rate is small and the kinematic range considered for associates actually involves mostly true associates. This condition is easily satisfied in p-p collisions but is typically violated in high-energy A-A collisions, unless trigger particles are selected in a very high  $p_T$  ranges.

# **Correlation Function Scaling**

By construction as a two-particle cumulant, the correlation function  $C_2(\Delta \phi)$  is expected to scale in proportion to the number of "sources," while  $R_2(\Delta \phi)$  should be inversely proportional to this number. For a collision system consisting of m independent identical sources, one should consequently get

$$C_2^{(m)}(\Delta\phi) = mC_2^{(1)}(\Delta\phi) \tag{11.24}$$

$$R_2^{(m)}(\Delta\phi) = \frac{1}{m}R_2^{(1)}(\Delta\phi). \tag{11.25}$$

The triggered correlation  $C_{T,A}$  has yet a different scaling property. If the number of trigger and associate particles are truly rare, both the numerator and the denominator of  $C_{T,A}$  are

expected to scale in proportion to the number of particle sources, and their ratio should consequently be invariant under variations of this number. In practice, particularly in heavy-ion collisions, both the number of trigger and associates can become rather large in central collisions, and this simple scaling is therefore violated. However, many researchers attempt to recover this property by removing combinatorial and collective correlation backgrounds using a technique known as zero yield at minimum (ZYAM) [16]. This technique assumes a two-component (two sources) particle production model, which may be approximately valid in the study of jets, provided the coupling (correlation) between the jet and the underlying background is small. This hypothesis may, however, be difficult to justify in analyses seeking to study the influence of the medium (bulk of produced particles) on the produced jets. It is thus preferable and logically consistent to define triggered correlation functions on the basis of  $C_2(\Delta\phi)$  rather than  $\rho_2(\Delta\phi)$  (see Problem 11.11).

# 11.1.2 Two-Particle $\Delta \eta$ Correlation Functions

Correlation functions measured in terms of the pseudorapidity difference of produced particles provide another powerful tool to explore the collision dynamics of both elementary particle and nuclear collisions. They have been used extensively, in particular, to study hadron production in p—p collisions and jet production in heavy-ion collisions.

As for the azimuthal correlations discussed in the previous section, we proceed to define two-particle correlation functions vs.  $\Delta \eta$  in terms of two-particle cumulants and normalized cumulants, as defined by Eq. (10.22),

$$C_2(\eta_1, \eta_2) = \rho_2(\eta_1, \eta_2) - \rho_1(\eta_1)\rho_1(\eta_2) \tag{11.26}$$

$$R_2(\eta_1, \eta_2) = \frac{\rho_2(\eta_1, \eta_2)}{\rho_1(\eta_1)\rho_1(\eta_2)} - 1. \tag{11.27}$$

The  $\eta_1$  vs.  $\eta_2$  dependence of these functions cannot, however, be readily reduced to a single variable  $\Delta\eta$ , such as in the case of azimuthal correlations. Indeed, it is quite possible that the correlation dynamics may be an arbitrary function of both  $\eta_1$  and  $\eta_2$ . In fact, measurements conducted in p-p collisions at the ISR and in p- $\bar{p}$  collisions at the Tevatron have shown that correlation functions may have a rather intricate dependence on both  $\eta_1$  and  $\eta_2$ , particularly when the particles have rapidities approaching the beam rapidity [85, 193]. However, in collider experiments with a focus on central rapidities ( $\eta \approx 0$ ), one may expect the correlations to depend primarily on the rapidity difference of the two particles considered, it is thus reasonable to recast the  $C_2$  and  $R_2$  correlation functions in terms of variables  $\Delta \eta = \eta_1 - \eta_2$  and  $\bar{\eta} = (\eta_1 + \eta_2)/2$ , average out the dependence on  $\bar{\eta}$ , and obtain correlation functions in terms of  $\Delta \eta$  exclusively. One must, however, properly account for the finite acceptance of the detector.

As an example, let us assume, as illustrated in Figure 11.6, that both particle 1 and 2 are measured in the same range  $-\eta_0 \le \eta < \eta_0$ , and let us calculate the two-particle cumulant  $C_2(\Delta \eta)$  assuming the cumulant  $C_2(\eta_1, \eta_2)$  is known. Averaging out over  $\bar{\eta}$  may

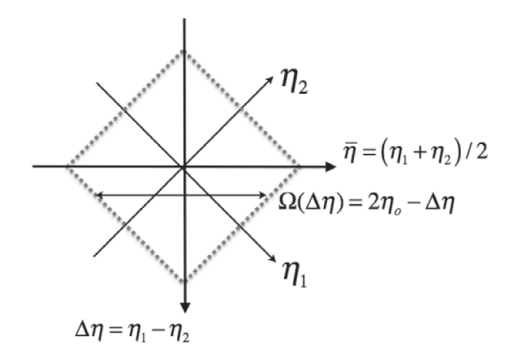


Fig. 11.6 Illustration of the rapidity acceptance of two-particle correlation measurements.

be accomplished as follows:

$$C_2(\Delta \eta) = \frac{1}{\Omega(\Delta \eta)} \iiint_{\Omega} C_2(\eta_1, \eta_2)$$

$$\times \delta(\Delta \eta - \eta_1 + \eta_2) \delta(\bar{\eta} - (\eta_1 + \eta_2)/2) d\eta_1 d\eta_2 d\bar{\eta},$$
(11.28)

where the factor  $\Omega(\Delta \eta)$  accounts for the width of the  $\bar{\eta}$  acceptance at a given value of  $\Delta \eta$ . For the square and symmetric acceptance illustrated in Figure 11.6, one gets

$$\Omega(\Delta \eta) = 2\eta_o - \Delta \eta. \tag{11.29}$$

This factor accounts for the fact that, with a square acceptance  $|\eta_i| < \eta_0$ , it is far less likely to observe pairs with a rapidity difference  $|\Delta \eta| \approx 2\eta_0$  than with  $\Delta \eta \approx 0$ . Failure to account for this simple geometric effect results in an apparently strong triangular correlation shape. The division by  $\Omega(\Delta \eta)$  is thus commonly known as the **triangle acceptance correction**. This is an unfortunate misnomer, however, because the division by  $\Omega(\Delta \eta)$  is not strictly speaking a correction of the data but a factor born out of the acceptance averaging over  $\bar{\eta}$ .

As for measurements of  $C_2(\Delta \phi)$ , two basic techniques, hereafter referred to as Method 1 (M1) and Method 2 (M2), may be used to obtain an estimator of  $C_2(\Delta \eta)$ .

M1 involves the determination of the two particle density  $\rho_2(\Delta \eta)$  directly using a 1D pair histogram,  $H_2$ , binned and filled at  $\Delta \eta = \eta_1 - \eta_2$  for all relevant pairs:

$$\hat{\rho}_2(\Delta \eta) = \frac{1}{\Omega(\Delta \eta)} \frac{k}{(N_{ev} - 1)\Delta_{\Delta \eta}} H_2(\Delta \eta). \tag{11.30}$$

The histogram  $H_2$  must be filled over all  $N_{ev}$  events satisfying relevant event cuts and all particle pairs satisfying track quality cuts and kinematic selection criteria of interest. The factor  $\Delta_{\Delta\eta}$  represents the bin width used to define and fill the histogram  $H_2$ . The factor k is unity for nonidentical particle pairs (e.g., kaons vs. pions, or particles in different  $p_T$  ranges), and equal to 2 for identical particles analyzed with two nested loops i < j over all particles (i.e., with  $1 \le i \le n_{\text{parts}}$  and  $i+1 < j \le n_{\text{parts}}$ ). The factor  $\Omega(\Delta\eta)$  must be determined numerically and accounts for the finite acceptance in  $\bar{\eta}$ .

The second term of the correlation function may be obtained by numerical integration of the product  $\hat{\rho}_1(\eta_1)\hat{\rho}_1(\eta_2)$ , where  $\hat{\rho}_1(\eta_i)$  is an estimator of the single particle density as a

function of  $\eta$ :

$$\hat{\rho}_1(\eta) = \frac{1}{(N_{ev})\Delta_{\eta}} H_1(\eta). \tag{11.31}$$

The factor  $\Delta_{\eta}$  represents the bin width used to fill the histogram  $H_1$ . Two distinct histograms  $H_1^{(1)}(\eta)$  and  $H_1^{(2)}(\eta)$  (and corresponding single particle densities) must obviously be used if the analysis is carried out on distinguishable particles. Numerical techniques to carry out the numerical integration of  $\hat{\rho}_1(\eta_1)\hat{\rho}_1(\eta_2)$  to obtain a function  $\hat{\rho}_1 \otimes \hat{\rho}_1(\Delta \eta)$  are discussed in §11.5. An estimator of  $\hat{C}_2(\Delta \phi)$  of the correlation function may thus be written

$$\hat{C}_2(\Delta\phi) = \hat{\rho}_2(\Delta\eta) - \hat{\rho}_1 \otimes \hat{\rho}_1(\Delta\eta). \tag{11.32}$$

One may alternatively estimate the second term  $\rho_1 \otimes \rho_1(\Delta \eta)$  of the correlation function on the basis of mixed events rather than a product of single particle densities. This is accomplished by filling 1D histogram  $H_2^{(\text{Mixed})}$  from pairs of particles obtained from mixed events. One then gets a mixed event density  $\hat{\rho}_2^{(\text{Mixed})}(\Delta \eta)$ 

$$\hat{\rho}_2^{\text{(Mixed)}}(\Delta \eta) = \frac{1}{\Omega(\Delta \eta)} \frac{k}{(N_{ev} - 1)\Delta_{\Delta \eta}} H_2^{\text{(Mixed)}}(\Delta \eta), \tag{11.33}$$

which should provide a legitimate estimate of the density product,  $\rho_1 \otimes \rho_1(\Delta \eta)$ , since particles produced in different collisions (events) should be physically uncorrelated. An estimator of  $\hat{C}_2(\Delta \phi)$  of the correlation function may thus also be obtained with

$$\hat{C}_2(\Delta \eta) = \hat{\rho}_2(\Delta \eta) - \hat{\rho}_2^{\text{(Mixed)}}(\Delta \eta). \tag{11.34}$$

Another approach, hereafter known as Method 2 (M2), consists of obtaining  $C_2(\Delta \eta)$  as an integral of  $C_2(\eta_1, \eta_2)$ . That is, one first obtains an estimate  $\hat{C}_2(\eta_1, \eta_2)$  based on histograms  $H_2(\eta_1, \eta_2)$  and  $H_1(\eta_i)$  accumulated over all relevant pairs of particles (tracks) and single particles, respectively, and estimate  $C_2$  as

$$\hat{C}_2(\eta_1, \eta_2) = \hat{\rho}_2(\eta_1, \eta_2) - \hat{\rho}_1(\eta_1)\hat{\rho}_1(\eta_2) \tag{11.35}$$

with

$$\hat{\rho}_1(\eta_i) = \frac{1}{N_{ev}\Delta_{\eta}} H_1(\eta_i), \tag{11.36}$$

$$\hat{\rho}_2(\eta_1, \eta_2) = \frac{1}{(N_{ev} - 1)\Delta_n^2} H_2(\eta_1, \eta_2), \tag{11.37}$$

where  $\Delta_{\eta}$  is the bin size used to define and fill histograms  $H_1$  and  $H_2$ . The estimator  $\hat{C}_2(\Delta \eta)$  is subsequently obtained by numerical integration of  $\hat{C}_2(\eta_1, \eta_2)$ 

$$\hat{C}_{2}(\Delta \eta) = \frac{1}{\Omega(\Delta \eta)} \sum_{\eta_{1}, \eta_{2}, \bar{\eta}} \hat{C}_{2}(\eta_{1}, \eta_{2})$$

$$\times \delta(\Delta \eta - \eta_{1} + \eta_{2}) \delta(\bar{\eta} - (\eta_{1} - \eta_{2})/2).$$
(11.38)

Alternatively, the term  $\hat{\rho}_1(\eta_1)\hat{\rho}_1(\eta_2)$  may be determined with pairs from mixed events:

$$\hat{\rho}_1(\eta_1)\hat{\rho}_1(\eta_2) = \frac{1}{(N_{ev} - 1)\Delta_\eta^2} H_2^{\text{(Mixed)}}(\eta_1, \eta_2), \tag{11.39}$$

Note that the use of finite width bins leads to a smearing of the correlation across the width of the  $\Delta \eta$  bin. Indeed, a specific bin in  $\Delta \eta$  obtained from two specific bins in  $\eta_1$  and  $\eta_2$  corresponds to an actual range  $\eta_1 - \eta_2$  which is larger than the width of the bin and effectively smears the correlation signal across bins.<sup>2</sup> This effect, often referred to as **aliasing**, can be reduced by oversampling the  $\rho_1(\eta_i)$  and  $\rho_2(\eta_1, \eta_2)$  distributions, in other words, by using bins in  $\eta$  that are two or more times smaller than the width  $\Delta \eta$ .

As for  $C_2$ , the normalized cumulant  $R_2(\Delta \eta)$  may in principle be determined with either M1 or M2. M1 estimates  $R_2(\Delta \eta)$  as the ratio

$$\hat{R}_2^{(M1)}(\Delta \eta) = \frac{\hat{C}_2(\Delta \eta)}{\hat{\rho}_1 \otimes \hat{\rho}_1(\Delta \eta)}$$
(11.40)

while M2 requires an average of  $\hat{R}_2(\eta_1, \eta_2)$  over  $\bar{\eta}$ :

$$\hat{R}_{2}^{(M2)}(\Delta \eta) = \frac{1}{\Omega(\Delta \eta)} \sum_{\eta_{1}, \eta_{2}, \bar{\eta}} \hat{R}_{2}(\eta_{1}, \eta_{2})$$

$$\times \delta(\Delta \eta - \eta_{1} + \eta_{2}) \delta(\bar{\eta} - (\eta_{1} + \eta_{2})/2).$$
(11.41)

Unfortunately, the two methods may yield substantially different results. Indeed, unlike the case of azimuthal correlations, for which the single densities  $\rho_1(\phi)$  are invariant under rotation in  $\phi$ , the single densities  $\rho_1(\eta_i)$  are arbitrary functions of  $\eta_i$ , that is, they may exhibit substantial variations throughout the acceptance of the measurement. This is a problem because the integral of the ratio of functions is in general not equal to the ratio of the integrals of these functions:

$$\int_{\Omega} \frac{\rho_2(\Delta \eta, \bar{\eta})}{\rho_1 \otimes \rho_1(\Delta \eta, \bar{\eta})} d\bar{\eta} \neq \frac{\int_{\Omega} \rho_2(\Delta \eta, \bar{\eta}) d\bar{\eta}}{\int_{\Omega} \rho_1 \otimes \rho_1(\Delta \eta, \bar{\eta}) d\bar{\eta}}$$
(11.42)

The issue may be exacerbated by detection inefficiencies that strongly depend on the coordinates  $\eta_1$  and  $\eta_2$ . This is discussed in detail in §12.4.3, where we argue that although less intuitive and direct from an experimental standpoint,  $R_2^{(M2)}(\Delta \eta)$  constitutes a more robust and meaningful measure of the normalized cumulant. In practice, at collider experiments, both the single particle  $\rho_1$  and pair densities  $\rho_2$  appear to have only rather modest dependence on rapidity in fiducial ranges measured. Constants can, of course, be factorized out of the preceding integrals and the two methods consequently yield very similar results in symmetric A–A collisions. Rapidity dependencies may, however, be larger in asymmetric collisions such as p–A collisions.

By construction as cumulants, the functions  $C_2$  and  $R_2$  exhibit the scaling properties embodied in Eqs. (10.25) and (10.39) discussed for generic cumulants in §10.2.4 and for azimuthal correlation functions in §11.1.1.

Triggered correlation functions  $C_{TA}(\Delta \eta)$  may be defined similarly to the functions  $C_{TA}(\Delta \phi)$  introduced §11.1.1. Caveats discussed for  $C_{TA}(\Delta \phi)$  apply to  $C_{TA}(\Delta \eta)$  also

<sup>&</sup>lt;sup>2</sup> For instance, combining yields from bins  $0.9 < \eta_1 \le 1.1$  and  $0.9 < \eta_2 \le 1.1$  corresponds to a range of  $-0.2 \le \eta_1 - \eta_2 \le 0.2$  being projected onto a  $\Delta \eta$  bin of width 0.2.

and are further complicated by issues associated with Method 1 discussed earlier. Precision measurements should be conducted exclusively with cumulants calculated based on Method 2.

The  $R_2(\Delta \eta)$  correlation function introduced in this section and the  $R_2(\Delta \phi)$  function introduced earlier can be trivially combined to obtain correlation functions with joint dependencies on  $\Delta \eta$  and  $\Delta \phi$ . Measurements with Method 2 yield

$$R_{2}^{(M2)}(\Delta \eta, \Delta \phi) = \frac{1}{\Omega(\Delta \eta)} \int_{\Omega} R_{2}(\eta_{1}, \phi_{1}, \eta_{2}, \phi_{2})$$

$$\times \delta(\Delta \eta - \eta_{1} + \eta_{2}) \delta(\bar{\eta} - (\eta_{1} + \eta_{2})/2) d\eta_{1} d\eta_{2} d\bar{\eta},$$

$$\times \delta(\Delta \phi - \phi_{1} + \phi_{2}) \delta(\bar{\phi} - (\phi_{1} + \phi_{2})/2) d\phi_{1} d\phi_{2} d\bar{\phi},$$
(11.43)

where

$$R_2(\eta_1, \phi_1, \eta_2, \phi_2) = \frac{\hat{\rho}_2(\eta_1, \phi_1, \eta_2, \phi_2)}{\hat{\rho}_1(\eta_1, \phi_1)\hat{\rho}_1(\eta_2, \phi_2)} - 1,$$
(11.44)

and the densities are obtained from multidimensional histograms filled by processing all relevant events and particles:

$$\hat{\rho}_1(\eta_i, \phi_i) = \frac{1}{N_{ev} \Delta_n \Delta_\phi} H_1(\eta_i, \phi_i), \tag{11.45}$$

$$\hat{\rho}_2(\eta_1, \phi_1, \eta_2, \phi_2) = \frac{k}{(N_{ev} - 1)\Delta_{\eta}^2 \Delta_{\phi}^2} H_2(\eta_1, \phi_1, \eta_2, \phi_2), \tag{11.46}$$

where, as in the preceding, k is unity for distinguishable particles and equal to 2 for indistinguishable particles analyzed with two-particle nested loops with an i < j condition.

#### 11.1.3 Balance Functions

The production of particles in elementary particles is constrained by energy/momentum conservation and several other conservation laws, such as charge conservation, baryon number conservation, and so on. A charge balance function provides a tool to emphasize effects associated with charge conservation on the charge particle production. For instance, in the case of pion production, one can assume that energy—momentum considerations affect the production of negative and positive pions in essentially the same way. However, one expects on general grounds that correlations between unlike-sign pions should be stronger than those between like-sign pions because charge conservation dictates that particles must be created in unlike-sign pairs. The charge balance function is designed to isolate the correlation strength associated with charge conservation specifically by measuring the number of unlike-sign pairs relative to the number of like-sign pairs in a given momentum volume. In heavy-ion collision studies, the charge balance function was also proposed by Bass et al. [31, 155] as a tool to identify the presence of a qualitative change in charged particle production versus collision centrality. The production of a long lived phase of quark gluon plasma, in particular, is expected to lead to delayed hadronization manifested by a

narrowing of the balance function measured as a function of the rapidity (or pseudorapidity) difference between produced particles [155].

The balance function introduced in ref. [31] is written

$$B(\Delta \eta) = \frac{\langle N_{-}N_{+}\rangle(\Delta \eta)}{\langle N_{-}\rangle} + \frac{\langle N_{+}N_{-}\rangle(\Delta \eta)}{\langle N_{+}\rangle} - \frac{\langle N_{+}(N_{+}-1)\rangle(\Delta \eta)}{\langle N_{+}\rangle} - \frac{\langle N_{-}(N_{-}-1)\rangle(\Delta \eta)}{\langle N_{-}\rangle},$$
(11.47)

where  $\langle N_-N_+\rangle(\Delta\eta)$ ,  $\langle N_+(N_+-1)\rangle(\Delta\eta)$ , and  $\langle N_-(N_--1)\rangle(\Delta\eta)$  represent the number of (+-), (++), and (--) pairs observed in a fixed range of pseudorapidity  $\Delta\eta$ , while  $\langle N_+\rangle$  and  $\langle N_-\rangle$  are the average numbers of positively and negatively charged particles detected in the measurement acceptance, respectively. Introducing normalized two-particle densities  $r_{\alpha,\beta}(\Delta\eta)$ , defined as

$$r_{\alpha,\beta}(\Delta \eta) = \frac{\langle N_{\alpha} N_{\beta} \rangle (\Delta \eta)}{\langle N_{\alpha} \rangle \langle N_{\beta} \rangle} \quad \text{for } \alpha \neq \beta$$

$$= \frac{\langle N_{\alpha} (N_{\alpha} - 1) \rangle (\Delta \eta)}{\langle N_{\alpha} \rangle^{2}} \quad \text{for } \alpha = \beta,$$
(11.48)

where the indices  $\alpha$  and  $\beta$  represent charges + and -, one may write the balance function as

$$B(\Delta \eta) = \langle N_{+} \rangle r_{-+}(\Delta \eta) + \langle N_{-} \rangle r_{+-}(\Delta \eta)$$

$$- \langle N_{+} \rangle r_{++}(\Delta \eta) - \langle N_{-} \rangle r_{--}(\Delta \eta).$$
(11.49)

At high collisional energy, one expects  $\langle N_+ \rangle \approx \langle N_- \rangle$  and  $r_{++}(\Delta \eta) \approx r_{--}(\Delta \eta)$  at central rapidities. Additionally, for a symmetric collision system (e.g., Pb + Pb), one also expects  $r_{-+}(\Delta \eta) = r_{+-}(\Delta \eta)$ . The balance function may then be expressed in terms of the charge-dependent correlation function,  $R_{CD}$ , defined in §10.7 (see also Problem 11.13).

$$B(\Delta \eta) = \langle N_{\rm ch} \rangle R_{\rm CD}(\Delta \eta) \tag{11.50}$$

where  $N_{ch} = N_+ + N_-$ . Use of this expression for a measurement of the balance function, rather than Eq. (11.47), has two obvious advantages: (1) the observable  $R_{\rm CD}$  is by construction robust against particle losses associated with detection efficiencies, and (2) the charge particle multiplicity has a simple dependency on detection efficiency that is usually simple to correct.

Pratt et al. have shown that the balance function is sensitive to radial flow effects that are independent and distinct from delayed hadronization effects. Radial flow effects may be modeled using a variety of techniques. The balance function thus constitutes an excellent observable to investigate the relative effects associated with charge transport (flow) and delayed hadronization [64]. The balance function (and related correlation functions) may be adapted to studies of net baryon number or net strangeness transport by substituting the number of baryons (strange particles) and anti-baryons (anti-strange) for the number of positively and negatively charged particles, respectively.

#### 11.1.4 Forward—Backward Correlations

The production of particles in elementary collisions at very high energy spans a very large range of rapidity. In order to understand the mechanisms that yield particles over such large range, researchers have sought to measure the correlation level between particles emitted forward and backward with a large rapidity gap. This type of correlation measurement is commonly known as **forward–backward correlation**. We first describe the technique in some detail, and next discuss its merits and limitations.

The forward–backward correlation technique essentially consists of a linear regression between the number of particles produced at **forward rapidities**, within a narrow range  $\delta\eta$  centered at  $+\eta$ , and the number of particles emitted at **backward rapidities**,  $-\eta$ , within an equivalent narrow range  $\delta\eta$ . Given fixed values of  $\eta$  and  $\delta\eta$ , one determines and plots the average number of particles produced forward,  $\langle n_F \rangle$ , for a given value (binned) of the number produced backward,  $n_B$ . One then fits the measured  $(n_B, \langle n_F \rangle)$  data points using a simple linear parameterization (i.e., a linear regression):

$$\langle n_F(n_B) \rangle = a + b \times n_B. \tag{11.51}$$

The measurement is repeated, and the coefficients a and b determined, for several values of the **rapidity gap**  $2\eta$ . The coefficient b, which describes the strength of the linear regression (i.e., the forward–backward correlation) may then be plotted as a function of the rapidity gap  $2\eta$ . While conceptually simple, the aforementioned measurement recipe is tedious of execution, and thus an alternative, more straightforward method is commonly used. This method relies on the hypothesis of a linear relationship between the particle yield emitted forward and backward. One writes

$$n_F - \langle n_F \rangle = b \times (n_B - \langle n_B \rangle) + r, \tag{11.52}$$

where b is the correlation strength to be determined, while r represents a random variable uncorrelated to the value of  $n_B$ , and with a vanishing expectation value,  $\langle r \rangle = 0$ . One may then calculate the expectation value of the product  $n_F n_B$  as follows:

$$\langle n_F n_B \rangle = b \left( \langle n_B^2 \rangle - \langle n_B \rangle^2 \right) + \langle n_F \rangle \langle n_B \rangle + \langle r n_B \rangle.$$
 (11.53)

Given r is assumed to be uncorrelated to  $n_B$ , the last term on the right vanishes, since  $\langle rn_B \rangle = \langle r \rangle \langle n_B \rangle$  and  $\langle r \rangle = 0$ . The slope coefficient b may consequently be written

$$b = \frac{\langle n_F n_B \rangle - \langle n_F \rangle \langle n_B \rangle}{\langle n_B^2 \rangle - \langle n_B \rangle^2},$$
(11.54)

which provides a simple and rapid method to determine the coefficient b in terms of the covariance,  $Cov[n_F, n_B] = \langle n_F n_B \rangle - \langle n_F \rangle \langle n_B \rangle$ , and the variance,  $Var[n_B] = \langle n_B^2 \rangle - \langle n_B \rangle^2$ .

Although the implementation of Eq. (11.54) is seemingly simple, accounting for detector effects, most particularly particle losses, is not. We will see in §12.4.2 that for measurements with limited efficiency,  $\epsilon$ , the variance of the particle multiplicity, n, detected in a given kinematical range scales as  $\epsilon^2 \text{Var}[n] + \epsilon n$ . The ratio b expressed by Eq. (11.54) consequently does not constitute a robust observable, and its correction to account for detection efficiencies, which may differ at forward and backward rapidity, is therefore not

trivial. However, since the information being sought lies within the strength of the covariance  $\langle n_F n_B \rangle - \langle n_F \rangle \langle n_B \rangle$ , a measurement of forward-backward correlation may then be obtained with a normalized two-particle cumulant:

$$C_{BF} = \frac{\langle n_F n_B \rangle - \langle n_F \rangle \langle n_B \rangle}{\langle n_F \rangle \langle n_B \rangle}$$
(11.55)

which is, by construction, robust under particle losses associated with detection efficiencies.

#### 11.1.5 Differential Transverse Momentum Correlations

Measurements of two- and multiple-particle correlations constitute powerful tools to study heavy-ion collision dynamics and enable the identification in nucleus—nucleus collisions of new correlation features not found in proton—proton interactions. These tools can be further enhanced by inserting weights dependent on the kinematical properties of the particles into the correlation function definition. We consider, as an example, the definition of two-particle differential transverse momentum correlation functions. As for integral transverse momentum fluctuation correlations (see §11.3.5), there is a certain latitude in the definition of such correlation functions. Indeed, as for integral correlations, one can use both **inclusive** and **event-wise** definitions [173]. One can also consider dynamical fluctuations as the difference between measured fluctuations and statistical fluctuations, that is, fluctuations expected for a purely Poisson system. Extension of the fluctuation variable  $\Phi_{p_T}$  [92, 146] is also possible. In this section, we use the notations introduced in prior sections and focus our discussion only on an **inclusive** definition. Extensions to event-wise and other differential fluctuation measures are also possible [173].

The  $\langle \Delta p_T \Delta p_T \rangle$  correlation function is defined as a **pair-averaged** product of deviates  $\Delta p_T \Delta p_T$ ,

$$\langle \Delta p_T \Delta p_T \rangle (\Delta \eta, \delta \phi) = \frac{1}{\Omega} \int_{\Omega} \frac{\rho_2^{(\Delta p_T \Delta p_T)}(\eta_1, \phi_1, \eta_2, \phi_2)}{\rho_2(\eta_1, \phi_1, \eta_2, \phi_2)} \times \delta(\Delta \eta - \eta_1 + \eta_2) \delta(\bar{\eta} - (\eta_1 + \eta_2)/2) \times \delta(\Delta \phi - \phi_1 + \phi_2) \delta(\bar{\phi} - (\phi_1 + \phi_2)/2) \times d\phi_1 d\eta_1 d\phi_2 d\eta_2 d\bar{\eta} d\bar{\phi}$$

$$(11.56)$$

where

$$\rho_2^{(\Delta p_T \Delta p_T)}(\eta_1, \phi_1, \eta_2, \phi_2) = \int_{\Omega} \rho_2(\vec{p}_1, \vec{p}_2) \times \Delta p_{T,1} \Delta p_{T,2} dp_{T,1} dp_{T,2},$$

$$\rho_2(\eta_1, \phi_1, \eta_2, \phi_2) = \int_{\Omega} \rho_2(\vec{p}_1, \vec{p}_2) dp_{T,1} dp_{T,2},$$
(11.57)

The function  $\rho_2(\vec{p_1}, \vec{p_2})$  is the pair density expressed with respect to the particles' rapidity, azimuth, and transverse momentum;  $\Delta p_{T,i} = p_{T,i} - \langle p_{T,i} \rangle$  and  $\langle p_{T,i} \rangle$  represents the inclusive average of the particle momenta in the fiducial acceptance of the measurement.

Given its explicit dependence on the product of deviates  $\Delta p_{T,1} \Delta p_{T,2}$ , the  $\langle \Delta p_T \Delta p_T \rangle$ correlation function provides a qualitatively different measure of particle correlations (relative to R<sub>2</sub>) that is sensitive to the particle momenta. Indeed, consider that a given pair of particles may involve two particles below the average momentum  $\langle p_{T,i} \rangle$ , two above, or one above and one below. The product  $\Delta p_{T,1} \Delta p_{T,2}$  may consequently be either positive or negative. A correlated particle pair involving two particles below (or above) the mean momentum will have a positive contribution to the correlation average, while correlated pairs consisting of one particle above and one particle below the momentum average should have a negative contribution to the correlation average. The  $\langle \Delta p_T \Delta p_T \rangle$  correlator thus provides a different way to probe particle production processes. For instance, processes such as Bose-Einstein condensation yield correlated pairs in close momentum proximity and should have a strong positive contribution to the  $\langle \Delta p_T \Delta p_T \rangle$  correlation function. On the other hand, particle decays that lead to the production of one slow particle and one highmomentum particle should have a negative contribution to  $\langle \Delta p_T \Delta p_T \rangle$ . The study of this correlation function thus provides an additional tool to probe and understand the particle production dynamics in elementary and nuclear collisions.

A measurement of  $\langle \Delta p_T \Delta p_T \rangle$  can be straightforwardly implemented using Method 2 discussed in §11.1.2. The average momentum should be obtained as an inclusive average over all particles of interest:

$$\langle p_{T,i} \rangle = \frac{1}{N_{\text{part}}} \sum_{\text{parts}} p_{T,i} \tag{11.58}$$

Estimates of the density  $\rho_2$  and weighted density  $\rho_2^{(\Delta p_T \Delta p_T)}$  may be obtained using four dimension histograms:

$$\hat{\rho}_2(\eta_1, \phi_1, \eta_2, \phi_2) = \frac{1}{N_{ev}} \frac{1}{\Delta_{\eta}^2 \Delta_{\phi}^2} H_2(\eta_1, \phi_1, \eta_2, \phi_2)$$
(11.59)

$$\hat{\rho}_2^{(\Delta p_T \Delta p_T)}(\eta_1, \phi_1, \eta_2, \phi_2) = \frac{1}{N_{ev}} \frac{1}{\Delta_{\eta}^2 \Delta_{\phi}^2} H_2^{(\Delta p \Delta p)}(\eta_1, \phi_1, \eta_2, \phi_2), \tag{11.60}$$

where  $H_2(\eta_1, \phi_1, \eta_2, \phi_2)$  is incremented by 1 at  $\eta_1, \phi_1, \eta_2, \phi_2$  for each pair measured while  $H_2^{(\Delta p \Delta p)}(\eta_1, \phi_1, \eta_2, \phi_2)$  is incremented by the product  $\Delta p_{T,1} \Delta p_{T,2}$ .

### 11.2 Three-Particle Differential Correlation Functions

Two-particle correlations enable a rather extensive study of particle correlations and have been instrumental in the study of jet production, flow, and several other phenomena encountered in both elementary and nuclear collisions at high-energy. At times, however, the interpretation of two-particle correlations may be somewhat ambiguous. For instance, in 2004, the PHENIX and STAR experiments reported two-particle correlation functions, with asymmetric  $p_T$  ranges (one high- and one low- $p_T$  particle), that indicated the

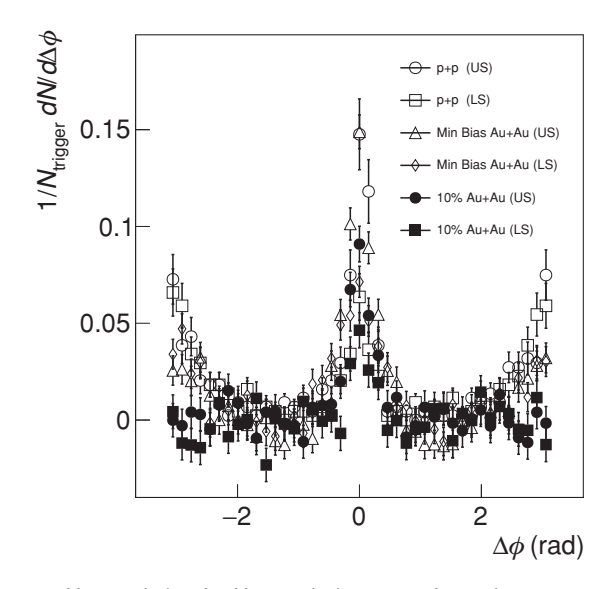


Fig. 11.7

Back-to-back suppression in like-sign (LS) and unlike-sign (UL) two-particle correlations measured in central (0–10%) Au + Au collisions relative to correlations measured in minimum-bias (Min Bias) Au+Au and in p-p collisions. Data from STAR collaboration. (Adapted from C. Adler, et al. Disappearance of back-to-back high pT hadron correlations in central Au+Au collisions at  $\sqrt{S_{NN}} = 200$ -GeV. *Physical Review Letters*, 90:082302, 2003.)

presence of a depletion in back-to-back emission at top RHIC energies, as illustrated in Figure 11.7 [11].

Theoretical analyses of these correlation functions suggested that several distinct production mechanisms might explain the suppressed and flattened away-side emission structure revealed by the two experiments. Unfortunately, the two-particle correlation measurements could not readily distinguish whether the broadening of the away-side was due to medium induced deflection of the leading partons with no actual broadening of the jet, or due to the interactions and dispersion of jet fragments by the medium, or due to a new phenomenon known as Mach cone emission, or perhaps another mechanism as yet unknown. Measurements of three-particle correlations were then conceived to attempt a resolution of this ambiguity.

If the jet structure is unchanged except for initial scattering of the leading jet parton, then the width of the away-side particles remains unchanged between p-p and Au + Au collisions. If, on the other hand, the jet fragments are dispersed (scattered) by the medium, then the width of the away-side should indeed increase, as schematically illustrated in Figure 11.8b. Three-particle azimuthal correlations could also be useful for identifying Mach cone emission or Cerenkov radiation. In the case of the predicted Mach cone emission, the propagation of the away-side parton in the dense medium formed by the A–A collisions was expected to lead to the production of a wake at an angle determined by the ratio of parton speed and sound velocity in the medium. There were predictions of a sound velocity of the order of 0.33c, whereas the parton speed is near c. This might then have led to particle emission at  $60-70^{\circ}$  from the away-side direction, as illustrated in Figure 11.8d, e.

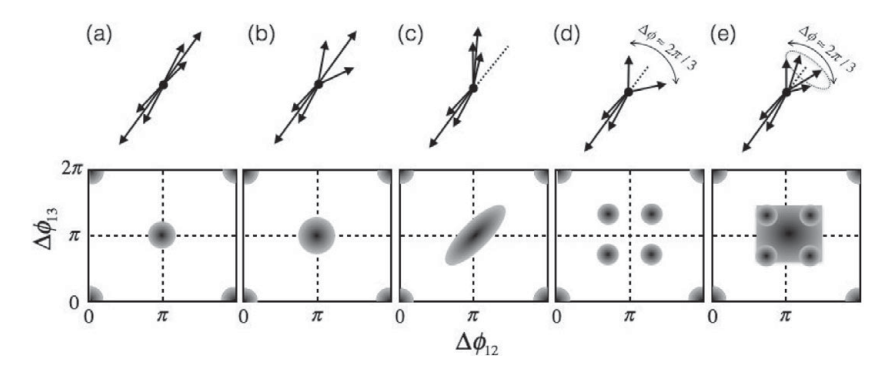


Fig. 11.8

Searching for Mach cone emission with three-particle correlations. Schematic illustration of three-particle azimuthal correlation patterns expected for (a) back-to-back jets; (b) medium induced broadening of the away-side jet; (c) deflected jets; (d) transverse plane emission of Mach cone; and (e) 3-D Mach cone.

Mach cone emission was then anticipated to yield four-side structures at  $60-70^{\circ}$  from the away-side direction, as schematically illustrated in Figure 11.8. In contrast, parton deflection (scattering) should have instead led to an elongation along the diagonal of the away-side jet peak (Fig. 11.8c). Measurements of three-particles were subsequently carried out by various groups to seek evidence for either of the correlated emission structures described earlier. Measurements by the STAR collaboration, in particular, involved a medium to high- $p_T$  particle, hereafter labeled as particle 1, and two lower  $p_T$  particles, labeled 2 and 3. Measurements were done in terms of the relative angles  $\Delta \phi_{12} = \phi_1 - \phi_2$  and  $\Delta \phi_{13} = \phi_1 - \phi_3$  between the particles.

Recall from §10.2 that measured *n*-particle densities involve combinatorial contributions from uncorrelated particle emission as well as correlated emission. It is thus strongly advisable to carry out an analysis based on normalized three-particle cumulants,  $R_3(\Delta\phi_{12}, \Delta\phi_{13})$  [158], which eliminate, by construction, combinatorial and uncorrelated triplets of the form  $\rho_1\rho_1\rho_1$  and  $\rho_2\rho_1$ . Normalized cumulants  $R_3$  also naturally lend themselves to particle-yield corrections required to account for instrumental effects, discussed in §12.4. In the context of the  $\Delta\phi_{12}$  vs.  $\Delta\phi_{13}$  three-particle correlation described earlier, the normalized cumulant  $R_3$  may be written:

$$R_3(\Delta\phi_{12}, \Delta\phi_{13}) = \frac{C_3(\Delta\phi_{12}, \Delta\phi_{13})}{\rho_1 \otimes \rho_1 \otimes \rho_1 \otimes \rho_1(\Delta\phi_{12}, \Delta\phi_{13})}.$$
 (11.61)

As for measurements of second-order normalized cumulants,  $R_2$ , one has the option of measuring  $R_3$  as function of  $\Delta\phi_{12}$  vs.  $\Delta\phi_{13}$  directly, using for instance a mixed-event technique, or via averages of  $R_3$  measured as functions of the three angles  $\phi_1$ ,  $\phi_2$ , and  $\phi_3$  explicitly. In this latter case, the cumulant  $C_3$  may be written

$$C_{3}(\phi_{1}, \phi_{2}, \phi_{3}) = \rho_{3}(\phi_{1}, \phi_{2}, \phi_{3}) - \rho_{2}(\phi_{1}, \phi_{2})\rho_{1}(\phi_{3})$$

$$- \rho_{2}(\phi_{1}, \phi_{3})\rho_{1}(\phi_{2}) - \rho_{2}(\phi_{2}, \phi_{3})\rho_{1}(\phi_{1})$$

$$+ 2\rho_{1}(\phi_{1})\rho_{1}(\phi_{2})\rho_{1}(\phi_{3}).$$

$$(11.62)$$

In practice, the determination of  $\rho_3(\phi_1, \phi_2, \phi_3)$  requires three dimensional histograms, and thus may be rendered difficult by the size of the dataset, or by computational and storage issues. One may therefore opt to determine the three-particle density directly in terms of the relative angles  $\Delta\phi_{12}$  and  $\Delta\phi_{13}$ . The determination of  $C_3$  then involves the computation of three terms  $\rho_2 \otimes \rho_1(\Delta\phi_{12}, \Delta\phi_{13})$  and  $\rho_1 \otimes \rho_1 \otimes \rho_1(\Delta\phi_{12}, \Delta\phi_{13})$ . Numerical techniques to estimate these terms on the basis of histograms with finitely many bins are discussed in §11.5. Direct estimations of  $\rho_3(\Delta\phi_{12}, \Delta\phi_{13})$  and terms of the form  $\rho_2(\Delta\phi_{ij})$  with 2D and 1D histograms, respectively, proceed with the same techniques as discussed in prior sections.

Three-particle correlation studies in pseudorapidities can be done, similarly, by substituting rapidities  $\eta_i$  to azimuthal angle  $\phi_i$  and differences  $\Delta \eta_{ij}$  to  $\Delta \phi_{ij}$  in Eq. (11.62). Note, however, that for correlation studies in rapidity (or pseudorapidity), no periodic boundary applies, and one must consequently consider the integration and averaging of the correlation functions over ranges  $\eta_{i,\min} - \eta_{j,\max} \leq \Delta \eta_{ij} < \eta_{i,\max} - \eta_{j,\min}$ . Numerical integration and averaging techniques are discussed in §11.5.

The interpretation of three-particle cumulants measured in heavy-ion collisions as functions  $\Delta\phi_{12}$  and  $\Delta\phi_{13}$  is greatly complicated by the presence of collective flow effects. Flow indeed contributes irreducible terms of the form  $\langle v_p(1)v_m(2)v_n(3)\rangle\delta_{p,m+n}cos(p\phi_1-m\phi_2-n\phi_3)$  to the cumulant that are functions of the product of three flow coefficients known to be dependent on the particle momentum and subject to fluctuations as well as correlations. A discussion of these terms is beyond the scope of this textbook but may be found in ref. [160].

# 11.3 Integral Correlators

#### 11.3.1 Introduction

Measurements of fluctuations in the relative production yields of two specific particle species are commonly performed to study the underlying particle production mechanisms and to investigate the nature of the system produced in elementary particle or nucleus–nucleus collisions. For example, it was predicted that event-by-event fluctuations of the ratio of the number of positively and negatively charged particles would be suppressed if a quark gluon plasma, as opposed to a hadron gas, were produced in high-energy nucleus-nucleus collisions. Similarly, fluctuations of the ratio of the yield of kaons to the yield of pions were also expected to be modified if the nuclear matter produced in collisions lies near a phase boundary or the critical point of nuclear matter. There also have been predictions and expectations for fluctuations of other types of particles or particle species.

While a measurement of event-by-event fluctuations of the ratio, R, of the yields of two particle types  $\alpha$  and  $\beta$  observed in a specific fiducial momentum range, hereafter denoted  $N_{\alpha}$  and  $N_{\beta}$ , may sound straightforward, complications may occur that make such measurements nontrivial. For instance, if the particle yields are small, there is a finite probability that the yield  $N_{\beta}$  may vanish in a given event, thereby leading to a divergent ratio

 $R = N_{\alpha}/N_{\beta}$ . Additionally, since particle detection efficiencies are typically functions of several kinematical and collision parameters, correcting the measured ratios for such fluctuations may become a rather complex task. Fortunately, a measurement of fluctuations of the ratio R may be replaced by an essentially equivalent measurement of two-particle integral correlators. Measurements of integral correlators are usually preferred relative to measurements of event-by-event fluctuations of particle yield ratios because they are not subject to divergences and can usually be corrected for detection efficiencies relatively easily. Integral correlators also present the advantage of being theoretically well defined and directly calculable. Their use for studies of relative yield fluctuations is consequently recommended over measurements of ratios.

# 11.3.2 Equivalence between Particle Yield Ratio Fluctuations and Integral Correlators

Let us first demonstrate the equivalence between measurements of ratio fluctuations and that of integral correlation functions. Let  $N_{\alpha}$  and  $N_{\beta}$  be the yields of two particle types (e.g., positively and negatively charged particles) measured in a given event within a fiducial momentum range. We are interested in measuring the variance  $\langle \Delta R^2 \rangle$  of the ratio  $R = N_{\alpha}/N_{\beta}$  of these two yields. Let  $\langle N_{\alpha} \rangle$  and  $\langle N_{\beta} \rangle$  represent event averages, that is, the expectation values of the yields  $N_{\alpha}$  and  $N_{\beta}$ . Let us further denote as  $\Delta N_{\alpha}$  and  $\Delta N_{\beta}$  the deviations of  $N_{\alpha}$  and  $N_{\beta}$  from their respective means, and define  $\langle R \rangle$  as the ratio of these averages. The ratio R may thus be written

$$R = \frac{\langle N_{\alpha} \rangle + \Delta N_{\alpha}}{\langle N_{\beta} \rangle + \Delta N_{\beta}}$$

$$= \langle R \rangle \left( \frac{1 + \Delta N_{\alpha} / \langle N_{\alpha} \rangle}{1 + \Delta N_{\beta} / \langle N_{\beta} \rangle} \right).$$
(11.63)

If the magnitude of the fluctuations  $\Delta N_i$  are small relative to the means  $\langle N_i \rangle$ , one can write

$$R = \langle R \rangle \left( 1 + \frac{\Delta N_{\alpha}}{\langle N_{\alpha} \rangle} - \frac{\Delta N_{\beta}}{\langle N_{\beta} \rangle} + O(1/N^2) \right). \tag{11.64}$$

The variance of the ratio normalized to the mean is thus

$$\frac{\langle \Delta R^2 \rangle}{\langle R \rangle^2} = \frac{\langle \Delta N_{\alpha}^2 \rangle}{\langle N_{\alpha} \rangle^2} + \frac{\langle \Delta N_{\beta}^2 \rangle}{\langle N_{\beta} \rangle^2} - 2 \frac{\langle \Delta N_{\alpha} \Delta N_{\beta} \rangle}{\langle N_{\alpha} \rangle \langle N_{\beta} \rangle}.$$
 (11.65)

The preceding quantity is commonly denoted  $\nu$  in the literature [161]. It may also be written

$$\nu \equiv \frac{\langle \Delta R^2 \rangle}{\langle R \rangle^2} = \left\langle \left( \frac{N_{\alpha}}{\langle N_{\alpha} \rangle} - \frac{N_{\beta}}{\langle N_{\beta} \rangle} \right)^2 \right\rangle. \tag{11.66}$$

In the limit of independent particle production (Poisson statistics), one expects that  $\langle \Delta N_i^2 \rangle = \langle N_i \rangle$  and the correlator  $\langle \Delta N_\alpha \Delta N_\beta \rangle$  vanishes. The so-called statistical limit of  $\nu$ , more aptly called the independent particle production limit, may thus be written

$$\nu_{\text{stat}} = \frac{1}{\langle N_{\alpha} \rangle} + \frac{1}{\langle N_{\beta} \rangle},\tag{11.67}$$

from which we find that the variance of the ratio fluctuations,  $\langle \Delta R^2 \rangle$ , becomes

$$\langle \Delta R^2 \rangle_{\text{stat}} = \nu_{\text{stat}} \langle R \rangle^2.$$
 (11.68)

Such statistical fluctuations are typically of limited interest because they are predominantly determined by the magnitude of the yields  $\langle N_{\alpha} \rangle$  and  $\langle N_{\beta} \rangle$ . Of greater interest is the deviation of  $\nu$  from the statistical limit  $\nu_{\rm stat}$ . One consequently introduces the difference  $\nu - \nu_{\rm stat}$ , known in the recent literature as a measure of dynamical fluctuations, noted  $\nu_{\rm dyn}$ . It is straightforward (Problem 11.1) to verify that

$$\nu_{\rm dyn} = \frac{\langle N_{\alpha}(N_{\alpha} - 1)\rangle}{\langle N_{\alpha}\rangle^2} + \frac{\langle N_{\beta}(N_{\beta} - 1)\rangle}{\langle N_{\beta}\rangle^2} - 2\frac{\langle N_{\alpha}N_{\beta}\rangle}{\langle N_{\alpha}\rangle\langle N_{\beta}\rangle}.$$
 (11.69)

This measure of fluctuations is of particular interest because the three terms it comprises are related to integral correlators  $R_{\alpha\beta}$ , as follows:

$$R_{\alpha\alpha} = \frac{\langle N_{\alpha}(N_{\alpha} - 1) \rangle}{\langle N_{\alpha} \rangle^{2}} - 1,$$

$$R_{\alpha\beta} = \frac{\langle N_{\alpha}N_{\beta} \rangle}{\langle N_{\alpha} \rangle \langle N_{\beta} \rangle} - 1.$$
(11.70)

The number of particle pairs  $\langle N_{\alpha}(N_{\alpha}-1)\rangle$  and  $\langle N_{\alpha}N_{\beta}\rangle$  are given by integrals of the particle production cross sections

$$\langle N_{\alpha}(N_{\alpha}-1)\rangle = \int_{\Omega} \rho_{\alpha\alpha} d\eta_1 d\phi_1 dp_{T,1} d\eta_2 d\phi_2 dp_{T,2}, \qquad (11.71)$$

$$\langle N_{\alpha}N_{\beta}\rangle = \int_{\Omega} \rho_{\alpha\beta} \, d\eta_{\alpha} d\phi_{\alpha} dp_{T,\alpha} d\eta_{\beta} d\phi_{\beta} dp_{T,\beta}, \qquad (11.72)$$

and the average single particle yields are given by

$$\langle N_{\alpha} \rangle = \int_{\Omega} \rho_{\alpha} \, d\eta_{\alpha} d\phi_{\alpha} dp_{T,\alpha}. \tag{11.73}$$

The quantities  $\rho_{\alpha}$  and  $\rho_{\alpha\beta}$  are single- and two-particle densities, respectively:

$$\rho_{\alpha}(\eta_{\alpha}, \phi_{\alpha}, p_{T,\alpha}) = \frac{d^{3}N}{d\eta_{\alpha}d\phi_{\alpha}dp_{T,\alpha}},$$
(11.74)

$$\rho_{\alpha\beta}(\eta_{\alpha}, \phi_{\alpha}, p_{T,\alpha}, \eta_{\beta}, \phi_{\beta}, p_{T,\beta}) = \frac{d^{6}N}{d\eta_{\alpha}d\phi_{\alpha}dp_{T,\alpha}d\eta_{\beta}d\phi_{\beta}dp_{T,\beta}}.$$
 (11.75)

The integrals may be taken over the entire acceptance of the detector or across specific narrow ranges in rapidity, production azimuth, and transverse momentum deemed suitable for the study of specific particle production mechanisms (e.g., emphasis on low- or high- $p_T$  particles).

Clearly, the integral correlators,  $R_{\alpha\beta}$ , are in all ways similar to the differential correlation functions introduced earlier in this chapter, and consequently sharing the same attributes and properties. They scale as the inverse of the multiplicities  $N_{\alpha}$ , and particle production by m distinct and independent sources (or mechanisms) should satisfy

$$R_{\alpha\beta}^{(m)} = \frac{1}{m} R_{\alpha\beta}^{(1)},$$
 (11.76)

where  $R_{\alpha\beta}^{(1)}$  and  $R_{\alpha\beta}^{(m)}$  are the correlators for a single process and a superposition of m identical such processes, respectively (see Problem 11.2). Integral correlators are also robust observables, i.e., observables independent of detection and measurement efficiencies – at least to first-order approximation, as we shall discuss in detail in §12.4. This implies, by construction, that the observable  $\nu_{\rm dyn}$  also shares these characteristics. One expects in particular that  $\nu_{\rm dyn}$  should scale as 1/m for nuclear collisions consisting of superpositions of m independent proton-proton (or perhaps parton–parton) processes (see Problem 11.3):

$$v_{\rm dyn}^{(m)} = \frac{1}{m} v_{\rm dyn}^{(1)}.$$
 (11.77)

Note, on the other hand, that the observable  $\nu = \langle \Delta R^2 \rangle / \langle R \rangle^2$  is not a robust observable given its explicit dependence on  $\langle N_{\alpha} \rangle$  and  $\langle N_{\beta} \rangle$  in the independent-particle production limit. Measurements of yield fluctuations are thus best conducted in terms of the robust variable  $\nu_{\rm dyn}$ , which provides a simple and explicit connection to two-particle densities and is as such easily interpreted.

Obviously, Eq. (11.64) is an approximation strictly valid only for small deviations  $\Delta N_i$  relative to the averages  $\langle N_\alpha \rangle$ . The correlator method discussed earlier is thus not an exact substitute for measurements of fluctuations of the ratios of particle species yields. Nonetheless, it remains the preferred observable given that (1) it does not suffer from the pathological behavior (divergence) associated with a ratio of numbers that may vanish, and (2) its interpretation in terms of integral correlators provides a strong and clear foundation for the interpretation of data.

In the following subsections, we discuss specific implementations of the  $\nu_{dyn}$  observable for the study of net charge fluctuations, and fluctuations of particle production.

# 11.3.3 Net Charge Fluctuations

Although electric charge is a conserved quantity, particle production in elementary particle and nuclear collisions is subject to net charge fluctuations. The net charge of particles produced in a given region of momentum space is expected to fluctuate collision by collision. The size of the fluctuations should be in part determined by the magnitude of the charge of the produced particles. In a quark gluon plasma (QGP), the charge carriers, the quarks, have fractional charges  $(\pm 1/3, \pm 2/3)$ , and therefore fluctuations of net charge should be suppressed relative to particle production in a hadron gas where charge carriers have integer charges  $(\pm 1)$ . Several theoretical works published in the 1990s in fact predicted that a signature of the production of QGP phase in relativistic heavy-ion collisions could be a substantial reduction of net charge fluctuations relative to that observed in lower energy collisions systems where no QGP is expected to be formed [46, 120, 121]. Subsequently, in the mid-2000s, several measurements were undertaken to find evidence for the predicted suppression of net charge fluctuations by SPS and RHIC experiments. Measurements of net charge fluctuations have also been conducted more recently at the LHC. While the results were somewhat inconclusive, the correlation functions developed to carry out the measurements have merits that extend beyond the search for explicit manifestation of the quark gluon plasma, and as such remain of general interest for the study of particle production dynamics in high-energy nuclear collisions.

The question arises as to what constitutes a reliable and significant measure of fluctuations of the net charge,  $Q = N_+ - N_-$  (for a review, see [157]). Clearly, the size of the fluctuations must depend on the actual produced particle multiplicity, the magnitude of the individual charges, as well as the efficiency of the counting and detection processes. A measurement of the variance of the produced multiplicity would therefore be incomplete and inconclusive. A measurement of the ratio  $N_+/N_-$ , however, would obviously be sensitive to fluctuations of the net charge. Alternatively, one might also consider the variance of Q relative to the average total number of charge particles  $\langle N_{\rm ch} \rangle = \langle N_+ \rangle + \langle N_- \rangle$ :

$$\omega_{Q} \equiv \frac{\langle \Delta Q^{2} \rangle}{\langle N_{+} \rangle + \langle N_{-} \rangle} = \frac{\langle Q^{2} \rangle - \langle Q \rangle^{2}}{\langle N_{ch} \rangle}.$$
 (11.78)

It is straightforward (see Problem 11.4) to show that one expects  $\omega_Q=1$ , for a strictly Poissonian system. Particle production is, however, not a perfect Poisson process. For instance, Koch et al.[120] estimated that the production of resonances, such as the  $\rho$ -meson, in a hadron gas would reduce the fluctuations to  $\omega_Q=0.8$ . They further predicted that a drastic reduction to  $\omega_Q=0.2$  would take place in the presence of a quickly expanding QGP [46, 121].

Inspection of the expressions for  $\omega_Q$  reveals that this observable depends linearly on the efficiency,  $\epsilon$ , of the detection and particle counting process. Because the efficiency may depend on the particle species considered as well as various other factors such as the detector occupancy, environmental features, defective detector components, and so on, the normalized variance constitutes a nonrobust observable, that is, one which requires a detailed calculation of the detection efficiency involving the various characteristics (flaws) and cuts used in the analysis. It is thus of interest to seek observables that are sensitive to net charge fluctuations but remain robust under practical experimental conditions. An obvious choice is the dynamic fluctuation observable,  $\nu_{\rm dyn}$ , introduced in the previous section. Let  $N_\alpha = N_+$  and  $N_\beta = N_-$ , one gets

$$\nu_{+-,\text{dyn}} = \frac{\langle N_{+}(N_{+}-1)\rangle}{\langle N_{+}\rangle^{2}} + \frac{\langle N_{-}(N_{-}-1)\rangle}{\langle N_{-}\rangle^{2}} - 2\frac{\langle N_{+}N_{-}\rangle}{\langle N_{+}\rangle\langle N_{-}\rangle}.$$
 (11.79)

The quantities  $\langle N_+(N_+-1)\rangle$ ,  $\langle N_-(N_--1)\rangle$ , and  $\langle N_+N_-\rangle$  are the average number of positively charged, negatively charged, and unlike-sign pairs, respectively, measured within a fiducial momentum volume over an ensemble of events.  $\langle N_+\rangle$  and  $\langle N_-\rangle$  are the average yields of positive and negative particles averaged over the same fiducial volume and event ensemble.  $\nu_{+-,\rm dyn}$  shares all attributes and properties of  $\nu_{\rm dyn}$  correlation functions. It is determined by the integral correlators  $R_{++}$ ,  $R_{--}$ , and  $R_{+-}$  and is as such a robust observable.

 $\nu_{+-,dyn}$  may be measured as a function of global event observables such as the total transverse energy or the charged particle multiplicity produced in a selected part of the experimental acceptance. However, care must be taken to correct for finite bin width effects as discussed in §12.4.3.

Measurements of correlation functions in elementary particle collisions at the ISR, the Tevatron (FNAL), the SPS (CERN), and RHIC (BNL) have shown that  $R_{++} \approx R_{--} < R_{+-}/2$  [85, 193]. The dynamic fluctuations  $\nu_{+-,\rm dyn}$  are consequently found to be negative

in such elementary processes. They are also found to be negative in nucleus–nucleus collisions, where  $\nu_{+-,dyn}$  roughly scales inversely as the produced particle multiplicity [3, 159].

Charge conservation fixes the total charge produced in an elementary particle (or nuclear) collision. A measurement encompassing all particles produced by a collision (i.e., over  $4\pi$  acceptance and perfect detection efficiency) would thus not be subject to net charge fluctuations. Particle production at SPS, RHIC, and LHC, however, spans several units of rapidity, and it is typically not possible to measure the full range of produced particles. Net charge fluctuations do take place on the scale of few units of rapidity. The strength of such fluctuations should in fact be sensitive to the degrees of freedom (i.e., hadronic vs. partonic) of the matter produced in high-energy collisions. Charge conservation does impact the measured fluctuations. One finds [157] that charge conservation yields a contribution to  $\nu_{+-,\rm dyn}$  on the order of

$$v_{+-,\text{dyn}}^{cc} = -\frac{4}{\langle N \rangle_{4\pi}},\tag{11.80}$$

where the superscript cc indicates the "charge conservation" limit, and  $\langle N \rangle_{4\pi}$  is the average total charged particle multiplicity produced by a collision system at a given impact parameter in nucleus–nucleus collisions (see also [46]).

Several other fluctuation observables have been proposed and used to measure net charge fluctuations. Of particular note is the  $\Phi_q$  observable, specifically designed to identify dynamic fluctuations of the net charge [92] produced in nucleus–nucleus collisions. By construction,  $\Phi_q$  yields a constant value for nucleus–nucleus collisions that could be reduced to a superposition of independent proton–proton interactions. It thus enables, at least in principle, identification of not only dynamic fluctuations, but fluctuations that might vary nontrivially as a function of collision system size, or collision centrality relative to proton–proton interactions. However, one can show that  $\Phi_q$  can be expressed in terms of  $\nu_{+-,\rm dyn}$  [157], as follows:

$$\Phi_q \approx \frac{\langle N_+ \rangle^{3/2} \langle N_- \rangle^{3/2}}{\langle N \rangle^2} \nu_{+-,\text{dyn}}.$$
(11.81)

Given its explicit dependence on particle multiplicities, one concludes this observable is nonrobust against particle detection efficiencies. Use of the observable  $\nu_{+-,dyn}$  is consequently recommended for practical measurements of net charge fluctuations. Changes in the collision dynamics may then be identified by scaling  $\nu_{+-,dyn}$  with the produced charged particle multiplicity (corrected for detection efficiencies and charge conservation effects).

#### 11.3.4 Kaon vs. Pion Yield Fluctuations

Anomalous fluctuations in the yield of kaons, relative to the yield of (charged) pions, were suggested as a potential signature of the formation of a quark gluon plasma in high-energy heavy-ion collisions [49]. Several measurements of such fluctuations have been conducted at the SPS (CERN) in terms of the variance,  $\Delta R^2$ , of the ratio of the yield of charged kaons

and charged pions measured in fixed rapidity and momentum ranges,

$$R = \frac{N_K}{N_{\pi}},\tag{11.82}$$

relative to the mean ratio

$$\langle R \rangle = \frac{\langle N_K \rangle}{\langle N_\pi \rangle}.\tag{11.83}$$

Given that  $\Delta R^2$  is sensitive to trivial statistical fluctuations, as well as actual correlations in the particle production of kaons and pions, measurements in terms of this variable typically rely on a comparison of the variance measured in actual events (siblings) relative to those found in mixed events. Such a comparison is complicated, however, by various detector effects, and most particularly, by detection efficiencies.

In light of the discussion in §11.3.2, which establishes an equivalence between the dynamical fluctuations measured with  $\nu_{\rm dyn}$  and deviations of the measured variance  $\Delta R^2$  from the independent particle limit, it is advisable to carry measurements of relative kaon and pion yields in terms of  $\nu_{\rm dyn}$ , which is by construction a robust quantity. Such measurements have been conducted at RHIC [4] in terms of the  $\nu_{\rm K\pi,dyn}$  observable, defined as:

$$\nu_{\mathrm{K}\pi,\mathrm{dyn}} = \frac{\langle N_K(N_K - 1) \rangle}{\langle N_K \rangle^2} + \frac{\langle N_\pi(N_\pi - 1) \rangle}{\langle N_\pi \rangle^2} - 2 \frac{\langle N_K N_\pi \rangle}{\langle N_K \rangle \langle N_\pi \rangle},\tag{11.84}$$

where  $\langle N_K(N_K-1)\rangle$  and  $\langle N_\pi(N_\pi-1)\rangle$  are second-order factorial moments of the produced kaon and pion yields, respectively,  $\langle N_K N_\pi \rangle$  represents the average number of kaon + pion pairs observed event-by-event in the fiducial acceptance, whereas  $\langle N_K \rangle$  and  $\langle N_\pi \rangle$  are the mean kaon and pion yields, respectively. This observable is by construction robust against particle loses associated with detection efficiencies. It is thus suitable to measure the rather small dynamical fluctuations observed in large multiplicity A–A collisions.

#### 11.3.5 Transverse Momentum Fluctuations

#### Introduction

Studies of event-by-event average transverse momentum fluctuations in heavy-ion collisions were initially undertaken to search for evidence of critical phenomena predicted to take place near the hadron–parton phase boundary and identify the formation of a quark gluon plasma [8, 9]. Although no conclusive evidence for the formation of a quark gluon plasma arose from early studies in Au–Au collisions, it was clear that transverse momentum fluctuations constituted a useful technique to study the collective dynamics of nucleus–nucleus collisions, most particularly radial flow effects. Studies were thus carried out by several groups for multiple colliding systems and at several colliding energies [6, 9, 12, 22, 104].

The event-wise mean transverse momentum is often defined as

$$\langle p_T \rangle \equiv \frac{1}{N} \sum_{i=1}^{N} p_{T,i}, \tag{11.85}$$

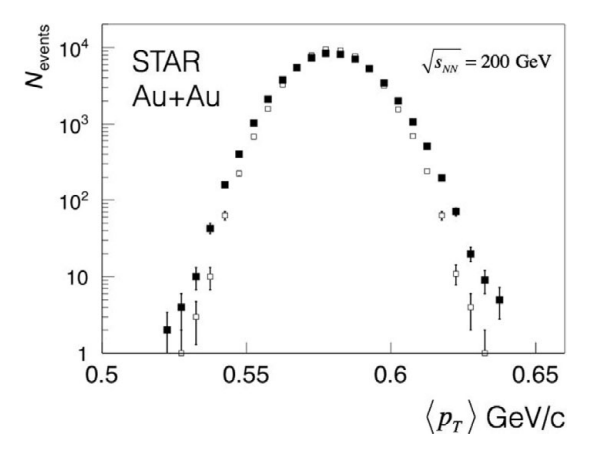


Fig. 11.9 Distribution of  $\langle p_T \rangle$  per event (solid squares) measured for 5% most central Au+Au collision at  $\sqrt{s_{NN}} = 200$  GeV, compared to a mixed event average  $p_T$  distribution (open squares). Data from STAR collaboration. (Adapted from J. Adams et al. Incident energy dependence of pt correlations at RHIC. *Physical Review C*72:044902, 2005.)

where N is the total number of particles per event detected in the kinematical range of interest and  $p_{T,i}$  represents their transverse momenta. The kinematical range may be selected in rapidity, azimuthal angle, and transverse momentum. The sum can in principle be carried on all detected particles, neutral or charged particles only, or some specific set of particle species. Figure 11.9 displays a measurement of the event-wise mean transverse momentum (Black squares) measured by the STAR collaboration in Au–Au collisions at  $\sqrt{S_{NN}} = 200$  GeV [9], compared to a mean  $p_T$  distribution (open squares) obtained with mixed events. Mixed events, defined in §12.4.5, are obtained by mixing particles from different events and thus carry no intrinsic particle–particle correlation. They thus constitute a sensible reference to establish whether particles produced in a given event do exhibit correlations. One finds that the mean  $p_T$  distribution of actual events is slightly wider than the reference histogram, which means that dynamic mean  $p_T$  fluctuations take place in Au–Au collisions, that is, fluctuations exceed the statistical fluctuations expected for a stochastic system consisting of independently produced particles.

An intuitive and quantitative measure of dynamical fluctuations is the excess variance,  $\delta p_t^2$ , of the data relative to the reference:

$$\delta p_t^2 = \sigma_{\text{data}}^2 - \sigma_{\text{ref}}^2 \tag{11.86}$$

where  $\sigma_{\rm data}^2$  and  $\sigma_{\rm ref}^2$  are the variance of the real and reference mean  $p_T$  distributions, respectively. However, in view of limited particle detection efficiencies, the measured mean  $p_T$  distributions (real and mixed events) may be subject to artificial broadening associated with purely instrumental effects. The  $\delta p_t^2$  observable also obscures the origins of the dynamical fluctuations, which are found in two- and multiparticle correlations. It is thus of greater interest to use observables that render this connection more explicit. Unfortunately, there exists several distinct ways to define and measure mean  $p_T$  observables that make this connection more explicit. Although qualitatively similar, the results obtained with these different definitions are found to be quantitatively distinct.

# $\langle \Delta p_T \Delta p_T \rangle$ Correlation Functions

In this section, we introduce the so-called **event-wise** (EW) and **inclusive** (I)  $\Delta p_T \Delta p_T$  observables. We show in the next section, that these observables can be both approximately related to the excess  $p_T$  variance defined by Eq. (11.86).

The event-wise average  $p_T$  per event is defined as

$$\langle \langle p_T \rangle \rangle_{EW} = \frac{1}{N_{\text{ev}}} \sum_{\alpha=1}^{N_{\text{ev}}} \frac{S_{\alpha}^{p_T}}{N_{\alpha}},$$
 (11.87)

where

$$S_{\alpha}^{p_{T}} = \sum_{k=1}^{N_{\alpha}} p_{T,k}, \tag{11.88}$$

which is the sum of the transverse momenta of the  $N_{\alpha}$  particles in event  $\alpha$ , and  $N_{\rm ev}$  is the number of events considered.

The inclusive average  $p_T$  is obtained by taking the event averages of  $S_{\alpha}^{p_T}$  and  $N_{\alpha}$  separately:

$$\langle \langle p_T \rangle \rangle_I = \frac{\frac{1}{N_{\text{ev}}} \sum_{\alpha=1}^{N_{\text{ev}}} S_{\alpha}^{p_T}}{\frac{1}{N_{\text{ev}}} \sum_{\alpha=1}^{N_{\text{ev}}} N_{\alpha}} = \frac{\sum_{\alpha=1}^{N_{\text{ev}}} S_{\alpha}^{p_T}}{\sum_{\alpha=1}^{N_{\text{ev}}} N_{\alpha}} \equiv \frac{\langle S^{p_T} \rangle}{\langle N \rangle}.$$
 (11.89)

While the definition of  $\langle \langle p_T \rangle \rangle_{EW}$  may seem more "intuitive," the inclusive definition has the advantage of being directly related to the particle production cross section, and is thus recommended. Noting that  $\sum S_{\alpha}^{p_T}$  is the sum of transverse momenta of all the particles measured in the data sample of interest, and that  $\sum N_{\alpha}$  is the total number of such particles, one can write

$$\langle \langle p_T \rangle \rangle_I = \frac{\sum_{\text{all}} p_T}{N_{\text{particles}}}.$$
 (11.90)

This expression is indeed just the average  $p_T$  of all the particles measured, and it can be written in terms of the inclusive single-particle cross section:

$$\langle \langle p_T \rangle \rangle_I = \frac{\int_{\Omega} \rho_1(\eta, \phi, p_T) p_T^2 \, d\eta d\phi dp_T}{\int_{\Omega} \rho_1(\eta, \phi, p_T) p_T \, d\eta d\phi dp_T}, \tag{11.91}$$

where the integration is taken over a selected subset  $\Omega$  of the detector's acceptance, and

$$\rho_1 = \frac{d^3N}{p_T \, d\eta d\phi dp_T}.\tag{11.92}$$

Writing a similar formula for  $\langle\langle p_T\rangle\rangle_{EW}$  is possible but yields a rather complicated expression in terms of conditional cross-sections (see, e.g., [173] and Problem 11.6). One however expects that the two definitions converge in the large N particle production limit.

The event-wise and inclusive  $\langle \Delta p_T \Delta p_T \rangle$  observables are defined as covariances relative to mean  $p_T$  averages, respectively. The event-wise  $\langle \Delta p_T \Delta p_T \rangle_{EW}$  is given by

$$\langle \Delta p_T \Delta p_T \rangle_{EW} = \frac{1}{N_{\text{ev}}} \sum_{\alpha=1}^{N_{\text{ev}}} \frac{S_{\alpha}^{\Delta p_T \Delta p_T}}{N_{\alpha}(N_{\alpha} - 1)}$$
(11.93)

with

$$S_{\alpha}^{\Delta p_T \Delta p_T} = \sum_{i=1}^{N_{\alpha}} \sum_{j=1, j \neq i}^{N_{\alpha}} (p_{T,i} - \langle \langle p_T \rangle \rangle_{EW}) (p_{T,i} - \langle \langle p_T \rangle \rangle_{EW}).$$
 (11.94)

The inclusive  $\langle \Delta p_T \Delta p_T \rangle_I$  is similarly given by

$$\langle \Delta p_T \Delta p_T \rangle_I = \frac{\sum_{\alpha=1}^{N_{\text{ev}}} S_{\alpha}^{\prime \Delta p_T \Delta p_T}}{\sum_{\alpha=1}^{N_{\text{ev}}} N_{\alpha}(N_{\alpha} - 1)} = \frac{\langle S^{\prime \Delta p_T \Delta p_T} \rangle}{\langle N(N - 1) \rangle}$$
(11.95)

with

$$S'_{\alpha}^{\Delta p_{T} \Delta p_{T}} = \sum_{i=1}^{N_{\alpha}} \sum_{j=1, j \neq i}^{N_{\alpha}} (p_{T,i} - \langle \langle p_{T} \rangle \rangle_{I}) \left( p_{T,j} - \langle \langle p_{T} \rangle \rangle_{I} \right). \tag{11.96}$$

As for  $\langle p_T \rangle_{EW}$ , the covariance  $\langle \Delta p_T \Delta p_T \rangle_{EW}$  may seem more intuitive because it involves an average of  $S_{\alpha}^{\Delta p_T \Delta p_T}$  calculated per pair of particles. The covariance  $\langle \Delta p_T \Delta p_T \rangle_I$  is, however, of greater interest because it can be expressed easily as an integral of the two-particle cross section:

$$\langle \Delta p_T \Delta p_T \rangle_I = \frac{\int_{\text{accept}} \rho_2 \Delta p_{T,i} \Delta p_{T,j} \, d\eta_1 d\phi_1 p_{T,1} dp_{T,1} d\eta_2 p_{T,2} d\phi_2 dp_{T,2}}{\int_{\text{accept}} \rho_2 \, d\eta_1 d\phi_1 p_{T,1} dp_{T,1} d\eta_2 d\phi_2 p_{T,2} dp_{T,2}}, \qquad (11.97)$$

with

$$\Delta p_{T,i} = p_{T,i} - \langle \langle p_T \rangle \rangle_I, \tag{11.98}$$

and

$$\rho_2 = \frac{d^6N}{p_{T,1}p_{T,2} d\eta_1 d\phi_1 dp_{T,1} d\eta_2 d\phi_2 dp_{T,2}}$$
(11.99)

Defined as a covariance,  $\langle \Delta p_T \Delta p_T \rangle_I$  features the same properties as regular correlation functions. It is a robust variable against particle losses due to detection efficiencies and it scales inversely as the produced particle multiplicity as well as the number of independent particle sources (see Problem 11.8).

Relation between 
$$\langle \Delta p_T \Delta p_T \rangle$$
 and  $\delta p_t^2$ 

We show that the excess variance,  $\delta p_t^2$ , defined by Eq. (11.86) can be expressed in terms of the correlator  $\langle \Delta p_T \Delta p_T \rangle$  by calculating the first and second moments of the sum  $S^{p_T}$  defined by Eq. (11.88).

For events with a fixed number of particles N, one can write

$$\langle S^{p_T} \rangle_N = \frac{1}{N} \left\langle \sum_{i=1}^N p_{T,i} \right\rangle = \frac{1}{N} \sum_{i=1}^N \langle p_{T,i} \rangle = \langle p_T \rangle$$

$$\langle S^{p_T} \rangle_N^2 = \frac{1}{N^2} \sum_{i=1}^N \langle p_{T,i} \rangle^2 + \frac{1}{N^2} \sum_{i \neq j=1}^N \langle p_{T,i} \rangle \langle p_{T,j} \rangle$$

$$\langle (S^{p_T})^2 \rangle_N = \frac{1}{N^2} \left\langle \left( \sum_{i=1}^N p_{T,i} \right) \left( \sum_{j=1}^N p_{T,j} \right) \right\rangle$$

$$= \frac{1}{N^2} \sum_{i=1}^N \langle p_T^2 \rangle + \frac{1}{N^2} \sum_{i \neq j=1}^N \langle p_{T,i} p_{T,j} \rangle.$$

$$(11.100)$$

The variance of  $S^{p_T}$ , for fixed N, is thus

$$\operatorname{Var}\left[S^{p_{T}}\right] = \langle (S^{p_{T}})^{2} \rangle_{N} - \langle S^{p_{T}} \rangle_{N}^{2}$$

$$= \frac{1}{N} \left( \langle p_{T}^{2} \rangle - \langle p_{T} \rangle^{2} \right) + \frac{1}{N^{2}} \langle S'_{\alpha}^{\Delta p_{T} \Delta p_{T}} \rangle.$$
(11.101)

First, note that the difference  $\langle p_T^2 \rangle - \langle p_T \rangle^2$  corresponds to the variance  $\sigma_{p_T}^2$  of the inclusive  $p_T$  distribution, in other words, that obtained by plotting a histogram of all measured particles  $p_T$  values. Second, note that  $\text{Var}[S^{p_T}]$  is actually the variance  $\sigma_{\text{data}}^2$  of the histogram (data) of  $S^{p_T}$  discussed in §11.3.5. Clearly, the variance of an histogram of  $S^{p_T}$  accumulated with mixed events should have the same exact structure except for the fact that none of the particles composing a mixed-event are correlated. This implies that the quantity  $\langle S'_{\alpha}^{\Delta p_T \Delta p_T} \rangle$  should be null for mixed events. The variance  $\text{Var}[S^{p_T}]$  of the mixed event spectrum is thus simply equal to  $\sigma_{p_T}^2$ . We conclude that the excess variance  $\delta p_t^2$  representing the difference between the same and mixed-event variance is equal to  $\frac{1}{N^2} \langle S'_{\alpha}^{\Delta p_T \Delta p_T} \rangle$ . One thus obtains the result

$$\delta p_t^2 = \frac{\langle N(N-1)\rangle}{N^2} \langle \Delta p_T \Delta p_T \rangle_I, \qquad (11.102)$$

which tells us that the excess variance is approximately equal to the integral correlator  $\langle \Delta p_T \Delta p_T \rangle_I$ . It should be noted, however, that while the quantity  $\langle \Delta p_T \Delta p_T \rangle_I$  is by construction robust against particle loss due to detector inefficiencies, the quantities  $\delta p_t^2$  and  $\sigma_{p_T}^2$  are not. It is consequently recommended to conduct  $p_T$  fluctuations studies on the basis of  $\langle \Delta p_T \Delta p_T \rangle_I$  rather than using a mixed-event technique and a combination of the observables  $\text{Var}[S^{p_T}]$ , and  $\delta p_t^2$  and  $\sigma_{p_T}^2$ . The use of  $\langle \Delta p_T \Delta p_T \rangle_I$  rather than  $\langle \Delta p_T \Delta p_T \rangle_{EW}$  is also deemed preferable because  $\langle \Delta p_T \Delta p_T \rangle_I$  maps straightforwardly onto the well-defined correlation integral (11.97), while  $\langle \Delta p_T \Delta p_T \rangle_{EW}$  yields a more convoluted expression in terms of conditional cross sections, expressed for fixed values of the event multiplicity.

#### 11.4 Flow Measurements

Measurements of the momentum anisotropy of the particles produced in heavy-ion collisions constitute a central component of the RHIC and LHC heavy-ion programs because they provide tremendous insight into the nature and properties of the matter formed in these collisions. Theoretical studies indicate that the momentum anisotropy of produced particles finds its origin in the initial asymmetry of the geometry of the matter produced in heavy-ion collisions. The development of collective motion, or flow, results in part from anisotropic pressure gradients, momentum transport, and differential particle energy loss through the medium. From a practical standpoint, it is convenient to distinguish the radial and azimuthal components of the collective motion. The radial component, known as radial flow, may be estimated based of momentum spectra and momentum correlations, while measurements of the azimuthal component, known as anisotropic flow or simply flow, are achieved via two- and multiparticle azimuthal correlation functions. Since the spatial anisotropies vanish rapidly as collision systems expand and evolve, anisotropic flow is generally considered to be self-quenching and thus expected to originate mostly from the early phases of collisions, essentially during the first few fm/c (i.e.,  $\sim 3 \times 10^{-24}$ ) of heavy-ion collisions. Flow measurements are thus particularly sensitive to the early phases of collisions and the nature of the high-temperature and high-density matter produced in relativistic heavy-ion collisions. Flow measurements are also increasingly carried out on simpler colliding systems, such as p-Pb or even p-p to find out whether the energy densities and gradients produced in these systems are sufficient to produce radial and anisotropic flow.

#### 11.4.1 Definition of Flow and Nonflow

Since the development of anisotropic flow is dependent on the initial geometry of collision systems, it is particularly important to clearly define the geometry and coordinates used to quantify measurements of flow.

Figure 11.10 presents a schematic illustration of the transverse profile of colliding nuclei and the participant region created by p–p interactions (which can be viewed as parton–parton or proton–proton interactions). Note that the use of a classical description (i.e., classical particle trajectories) of the nuclei profile is justified by the very high momentum of the colliding particles, which endows them with very short De Broglie wavelengths. The reaction plane is defined by the beam direction and the impact parameter vector consisting of a line joining the geometrical centers of the colliding nuclei. Particularly relevant for flow measurements is the azimuthal angle,  $\Psi_{RP}$ , of the reaction plane relative to some laboratory reference direction (not shown in the figure). The angle  $\Psi_{RP}$  cannot be dialed macroscopically nor observed directly and must consequently be inferred from the distribution of produced particles. All values of  $\Psi_{RP}$  are a priori equally probable; the probability of measuring a given value of  $\Psi_{RP}$  can thus be described as a uniform PDF in the range  $[0, 2\pi]$ . The initial anisotropic spatial geometry of the system causes anisotropic

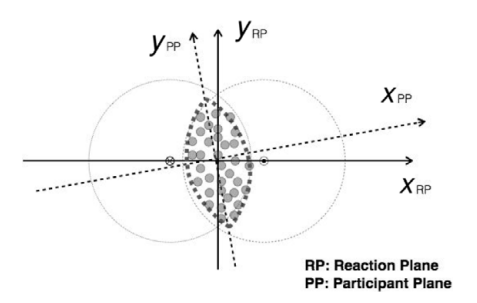


Fig. 11.10

The beam axis (extending out of page) and a line passing through the nuclei centers ( $x_{RP}$ ) define the nominal **reaction plane** (RP). Event-by-event fluctuations in the location of p-p (i.e., nucleon-nucleon or parton-parton) interactions define the participant region with axes of symmetry  $x_{PP}$  and  $y_{PP}$ . The beam and  $x_{PP}$  axes define the **participant plane** (PP).

pressure gradients and differential energy losses. As illustrated in Figure 11.6, the energy and pressure gradient are maximum along the x-axis, and one thus expects the largest particle production of low momentum particles subjected to flow gradients along this axis. High- $p_T$  particles produced during the earliest stages of a collision might not be driven by pressure gradients, but must nonetheless penetrate through the spatially anisotropic slower medium produced by the intersecting nuclei. Interactions with the medium are expected to produce energy losses. And since path lengths are shorter along the x-axis than along the y-axis, high- $p_T$  particles are expected to suffer differential energy losses. They too should exhibit azimuthal anisotropies. The particle production cross section is thus expected to depend on the azimuthal angle  $\phi$  relative to the orientation of the reaction plane  $\Psi$ . One may express this cross-section as a Fourier series:

$$E\frac{d^3N}{dp^3} = \frac{1}{2\pi} \frac{d^2N}{p_T dp_T dy} \left\{ 1 + 2 \sum_{n=1}^{\infty} v_n \cos\left[n\left(\phi - \Psi_{\text{RP}}\right)\right] \right\},\tag{11.103}$$

where the coefficients,  $v_n$ , are known as **flow coefficients** or simply as **harmonic coefficients**. The introduction of a factor of 2 in the preceding decomposition will be justified in the discussion that follows.

As in prior sections, it is convenient to define shorthand notations  $\rho_1(\phi, y, p_T)$  and  $\rho_1(y, p_T)$  for the single particle density,

$$\rho_1(\phi, y, p_T) = \frac{1}{2\pi} \rho_1(y, p_T) \left\{ 1 + 2 \sum_{n=1}^{\infty} v_n \cos\left[n\left(\phi - \Psi_{\text{RP}}\right)\right] \right\}$$
(11.104)

The flow coefficients,  $v_n$ , may be obtained as the expectation value of  $\cos [n(\phi - \Psi_{RP})]$ ,

$$v_n \equiv \langle \cos\left[n\left(\phi - \Psi_{\rm RP}\right)\right]\rangle \tag{11.105}$$

$$= \frac{\int_0^{2\pi} \rho_1(\phi, y, p_T) \cos[n(\phi - \Psi_{RP})] d\phi}{\int_0^{2\pi} \rho_1(\phi, y, p_T) d\phi}.$$
 (11.106)

The integral in the denominator of Eq. (11.106) yields  $\rho_1(y, p_T)$ . To carry out the integral in the numerator, with  $\rho_1(\phi, y, p_T)$  given by Eq. (11.104), recall the orthogonality relations

of cosine and sine functions,

$$\int_0^{2\pi} \cos(n\phi) \cos(m\phi) d\phi = \pi \delta_{nm}, \qquad (11.107)$$

$$\int_0^{2\pi} \sin(n\phi) \cos(m\phi) \, d\phi = 0, \tag{11.108}$$

defined for integer values of n, m > 0, and with the Kronecker delta function  $\delta_{nm} = 1$  for n = m, and null otherwise. One can thus verify easily that the integral in the numerator yields  $v_n \times \rho(y, p_T)$ . Note that the factor of 2 originally inserted in the definition of the Fourier decomposition multiplies the factor  $\pi$  obtained from the integral  $\int_0^{2\pi} \cos(n\phi) \cos(m\phi) \, d\phi$ . This consequently yields a factor  $2\pi$  that cancels the  $2\pi$  normalization factor of the invariant cross section. One concludes that the expectation value  $\langle \cos [n(\phi - \Psi_{\rm RP})] \rangle$  indeed yields the flow coefficients  $v_n$ . Further note that Eq. (11.105) produces flow coefficients, known as **differential flow coefficients**, that are dependent on the rapidity, y, and transverse momentum,  $p_T$ , of the particles. **Integrated flow coefficients**, also known as average flow coefficients, may be obtained by further integrating the particle density over the fiducial rapidity and transverse momentum acceptance of the measurements. Flow coefficients vanish at null  $p_T$  and grow approximately linearly at low  $p_T$  while the density  $\rho_1(y, p_T)$  is a steeply decreasing function at large  $p_T$ . Systematic errors associated with an integrated  $v_n$  measurement based on a finite  $p_T$  range can thus be controlled relatively easily.

Experimentally, the integrals in Eq. (11.105) are replaced by sums over all (or selected) particles measured in the fiducial acceptance. Given an estimate of the reaction plane angle,  $\hat{\Psi}_{RP}$ , one obtains flow coefficients with

$$v_n = \frac{\left\langle \sum_{i=1}^{N_p} \cos[n(\phi_i - \hat{\Psi}_{RP})] \right\rangle}{\langle N_p \rangle}, \tag{11.109}$$

where  $\phi_i$ , i = 1,  $N_p$ , are the azimuthal angles of measured particles and the sum runs over all  $N_p$  measured particles in any given event, and the brackets stand for an average over events. The  $v_n$  may be obtained in bins of  $p_T$  and y or integrated over the entire fiducial range of the measurement.

The Fourier decomposition used in Eq. (11.103) is obviously incomplete. Sine terms were omitted because, on average, there should be an equal number of particles produced below and above the reaction plane. Sine terms being odd in  $\phi - \Psi_{RP}$  are thus expected to vanish, on average, and are consequently not required for a description of the averaged particle emission relative to the reaction plane. Fluctuations in the number of particles, however, take place on an event-by-event basis. One might thus be tempted to introduce sine terms in the Fourier decomposition (11.103). It is, however, usually deemed more convenient and physically meaningful to describe collisions on event-by-event using the notion of **participant plane** illustrated in Figure 11.10.

The first four harmonic coefficients,  $v_1$ ,  $v_2$ ,  $v_3$ , and  $v_4$  are commonly known as **directed** flow, **elliptic flow**, **triangular flow**, and **quadrangular flow**, respectively, given their

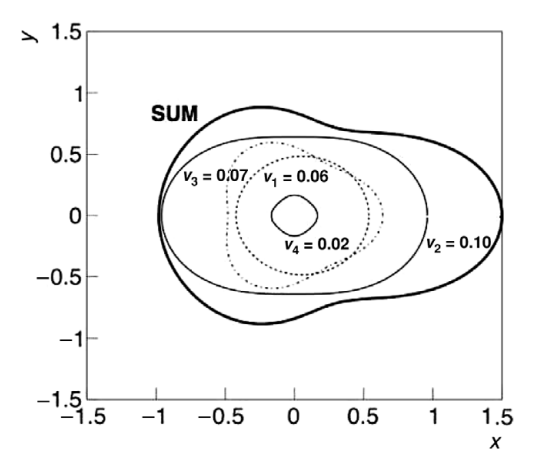


Fig. 11.11

Illustration of the geometrical interpretation of flow coefficients; the sizes of the radial profiles are plotted with  $r_n(\phi) = k_n(1 + 2v_n \cos(n\phi))$ , for given  $v_n$  values. The scaling coefficients  $k_n$  are set arbitrarily to facilitate the visualization of the different flow terms. The thick solid line represents a sum of the four terms.

obvious geometrical interpretation (Figure 11.11). Appellations in terms of dipole, quadrupole, and so on, should be frowned on since these names are usually reserved for the multipole expansion of three-dimensional charge or mass distributions, not the harmonic decomposition in azimuth of a flow field.

The reaction plane angle  $\Psi_{RP}$  is not readily accessible macroscopically but may be estimated based on the distribution of produced particles. Several of the techniques commonly used to estimate this angle and measure the flow coefficients based on two- and multiparticle correlation functions will be described in following sections and their relative merits discussed in §11.4.3. At this stage, it is important to point out that contributions to these correlation functions involving two- or *n*-particle correlations, resulting, for instance, from resonance decays or the production of jets, and having nothing to do with collective flow, may enter in the determination of flow coefficients. These contributions are commonly referred to as **nonflow**. They are noted  $\delta_n$  and can in principle be estimated from two-particle correlations based on the following expression:

$$\langle \cos[n(\phi_i - \phi_i)] \rangle = \langle v_n^2 \rangle + \delta_n. \tag{11.110}$$

Measurements of flow coefficients are further complicated by fluctuations of the magnitude of the flow on an event-by-event basis, all other collision properties being equal. The variations are known as **flow fluctuations**,  $\sigma_{vn}^2$ , and formally defined as the variance of the flow coefficients:

$$\sigma_{vn}^2 = \langle v_n^2 \rangle - \langle v_n \rangle^2. \tag{11.111}$$

From Eqs. (11.110) and (11.111), one gets:

$$\langle \cos[n(\phi_i - \phi_j)] \rangle = \langle v_n \rangle^2 + \sigma_{vn}^2 + \delta_n, \qquad (11.112)$$

which implies that measurements of  $\langle\cos[n(\phi_i-\phi_j)]\rangle$  are determined by the square of the magnitude of the (average) flow, the variance of the flow, as well as nonflow effects. It initially appeared that flow fluctuations might be inextricably linked to nonflow effects. Recent developments, however, suggest flow fluctuations may largely be determined by fluctuations in the overlapping nuclei geometry, known as the participant nucleons region. Theoretical considerations further suggest that the principal axes of the participant region may in fact deviate substantially from the nominal average overlap region, as schematically illustrated in Figure 11.10. The flow coefficients measured according to the participant plane are always larger than those obtained relative to the nominal reaction plane. This leads to important contributions to the flow fluctuations.

#### 11.4.2 Measurement Methods

In this section, we describe some of the many techniques developed over the years to estimate the flow coefficients  $v_n$ . These techniques vary in applicability based on the size of the data sample, ease of use, and their capacity to suppress or control nonflow effects.

## Standard Event Plane Method

The **standard event plane** method, also known simply as **event plane** (EP) method, is the most basic of all techniques used to determine flow coefficients. Defined by Eq. (11.105), it requires the estimation of the reaction plane angle,  $\Psi_{RP}$ , from the event plane computed on the basis of selected, or all, measured particles. The event plane determination proceeds on the basis of a 2D vector, denoted  $\vec{Q}_n$ , and known as the **event plane vector** of order n. It is calculated in the transverse plane, event-by-event, on the basis of the following expressions:

$$\vec{Q}_{n,x} = \sum_{i=1}^{N_p} w_i \cos(n\phi_i)$$
 (11.113)

$$\vec{Q}_{n,y} = \sum_{i=1}^{N_p} w_i \sin(n\phi_i).$$
 (11.114)

The sums run over the  $N_p$  measured particles. The  $\phi_i$ , with  $i=1,N_p$ , are the azimuthal angles of the measured particles in the laboratory reference frame. The coefficients  $w_i$  are weights assigned to each particle and designed to yield an optimal estimation of the event plane vector  $\vec{Q}_n$ , discussed in the text that follows. The event-plane angle,  $\Psi_n$ , and the modulus of  $\vec{Q}_n$  are obtained with

$$\hat{\Psi}_n = \frac{1}{n} \arctan\left(Q_n, y/Q_n, x\right) \tag{11.115}$$

$$|\hat{Q}_n| = \sqrt{Q_n, x^2 + Q_n, y^2}.$$
(11.116)

The weights,  $w_i$ , are positive definite for even values of n, but must satisfy  $w_i(-y) = -w_i(y)$  for odd harmonics. An optimal determination of the angle  $\Psi_n$  is achieved if the

weights are set equal to the flow coefficients,  $w_i = v_n(p_T, y)$  [182]. This is rather inconvenient because the  $v_n$  are not known a priori. It is, however, common and legitimate practice to use the  $p_T$  of the particles as weight, since the flow coefficients are typically proportional to the transverse momentum of the particles at low  $p_T$ . Estimates of the flow coefficients, noted  $v_n^{\text{obs}}$ , are obtained by replacing  $\hat{\Psi}_{\text{RP}}$  by  $\hat{\Psi}_n$  in Eq. (11.109),

$$v_n^{\text{obs}} = \left\langle \frac{1}{N_p} \sum_{i=1}^{N_p} \cos[n(\phi_i - \hat{\Psi}_n)] \right\rangle.$$
 (11.117)

Note that the orientation of the  $\vec{Q}$  vector is obviously influenced by the direction of all particles included in its calculation. As an extreme case, consider that if  $\vec{Q}$  was determined on the basis of a single particle, this particle's momentum vector would be perfectly aligned with it. This leads to an autocorrelation effect that tends to skew the  $\vec{Q}$  vector along the direction of high- $p_T$  particles (most particularly if a weight proportional to  $p_T$  is used), and as a result inappropriately increases the value of the flow coefficients. To avoid this auto-correlation bias, one must recalculate the vector  $\vec{Q}$ , for each particle included in the  $v_n$  calculation, to exclude the contribution of this particle to the flow vector. This may be written

$$v_n^{\text{obs}} = \left\langle \frac{1}{N_p} \sum_{i=1}^{N_p} \cos[n(\phi_i - \hat{\Psi}'_n)] \right\rangle,$$
 (11.118)

where  $\hat{\Psi}'_n$  is obtained, for each particle, from

$$\hat{\Psi}'_{n} = \frac{1}{n} \arctan(Q'_{n,y}/Q'_{n,x}), \tag{11.119}$$

with

$$\vec{Q}'_{n,x} = Q_{n,x} - w_i \cos(n\phi_i)$$
 (11.120)

$$\vec{Q}'_{n,v} = Q_{n,v} - w_i \sin(n\phi_i). \tag{11.121}$$

It is important to notice that for  $v_2$ , the definition (11.117) does not specify whether the anisotropy is in- or out-of-plane. Additional information, such as a measurement of the spectator plane using forward detectors, was required in practice to establish that the elliptic flow observed in heavy-ion collisions at RHIC and LHC energies is actually inplane. It also worth noting that, mathematically, there is no intrinsic or a priori relationship between the different angles  $\Psi_n$ . However, the geometry and dynamics of nuclei–nuclei collisions may impart a finite degree of correlation between these angles. Measurements of their covariance  $\text{Cov}[\Psi_m, \Psi_n]$  or average  $\cos(\Psi_m - \Psi_n)$  are thus of interest and provide valuable insight about the collision geometry and dynamics.

While the aforementioned procedure corrects for autocorrelation effects, it does not account for fluctuations associated with the finite number of particles. Indeed, one can show that Eq. (11.118) produces a biased estimator of the flow coefficient  $v_n$  because the event plane vector,  $\hat{Q}_n$ , randomly deviates from the actual reaction vector due to the finite particle multiplicity. For large multiplicities, the fluctuations of  $\hat{Q}_n$  can be shown to be Gaussian in the  $Q_x - Q_v$  plane, and thus the measured and true Fourier coefficients may be related by the

following expression: [151]

$$v_n^{\text{obs}} \equiv \langle \cos \left[ n \left( \phi - \Psi_{\text{RP}} \right) \right] \rangle \tag{11.122}$$

$$= \langle \cos [n(\phi - \Psi_n)] \rangle \times \langle \cos [n(\Psi_n - \Psi_{RP})] \rangle$$
 (11.123)

$$= v_n \times \langle \cos \left[ n \left( \Psi_n - \Psi_{\text{RP}} \right) \right] \rangle, \qquad (11.124)$$

from which we conclude that a correction for event plane resolution may be achieved with

$$v_n = \frac{v_n^{\text{obs}}}{R_n},\tag{11.125}$$

where the **event plane resolution**  $R_n$  is defined by

$$R_n = \langle \cos \left[ n \left( \Psi_n - \Psi_{\text{RP}} \right) \right] \rangle. \tag{11.126}$$

The event plane resolution coefficients  $R_n$  must be calculated for each harmonic n and obtained as an average taken over a large ensemble of events. Their magnitude depends on the strength of the flow  $v_n$  and the particle multiplicity M. They may be evaluated analytically if the  $\hat{Q}_n$  fluctuations are Gaussian according to [151]

$$R_n(\chi) = \frac{\sqrt{\pi}}{2} \chi e^{-\chi^2/2} \left[ I_{(n-1)/2}(\chi^2/2) + I_{(n+1)/2}(\chi^2/2) \right], \tag{11.127}$$

where  $\chi = v_n \sqrt{M}$ , and  $I_k$  are modified Bessel functions of order k. The functions  $R_n(\chi)$  are plotted in Figure 11.12 for k=1, k=2, and so on. Eq. (11.127) is useful to model the behavior of the event plane resolution relative to the strength of the flow coefficients and the particle multiplicity, but, it is not readily sufficient for the experimental determination of the event plane resolution.

The event plane resolution can be estimated directly from the data using the **subevent method**, which consists of randomly subdividing the particles of each measured event into two subevents A and B of (approximately) equal size M/2. One may then calculate the flow vectors  $\hat{Q}_n^A$  and  $\hat{Q}_n^B$  of the two subevents and determine the correlation  $\langle \cos[n(\hat{\Psi}_n^A - \hat{\Psi}_n^B)] \rangle$ . For Gaussian fluctuations and sufficiently large multiplicities, the two angles  $\hat{\Psi}_n^A$  and  $\hat{\Psi}_n^A$  are statistically independent, and one may consequently write

$$\langle \cos \left[ n (\hat{\Psi}_n^A - \hat{\Psi}_n^B) \right] \rangle = \langle \cos \left[ n (\hat{\Psi}_n^A - \hat{\Psi}_{RP}) \right] \rangle \times \langle \cos \left[ n (\hat{\Psi}_n^B - \hat{\Psi}_{RP}) \right] \rangle$$

$$= \langle \cos \left[ n (\hat{\Psi}_n^A - \hat{\Psi}_{RP}) \right] \rangle^2.$$
(11.128)

The event plane resolution of subevents A (or B) is thus

$$R_{n,\text{sub}} = \sqrt{\left\langle \cos\left[n(\hat{\Psi}_n^A - \hat{\Psi}_n^B)\right]\right\rangle}.$$
 (11.129)

The resolution for a full event may then be estimated from

$$R_{n,\text{full}} = R_n(\sqrt{2}\chi_{\text{sub}}). \tag{11.130}$$

The use of subevents is a powerful technique that enables a wide range of studies. One can produce subevents by random selection of particles of actual events, or on the basis of

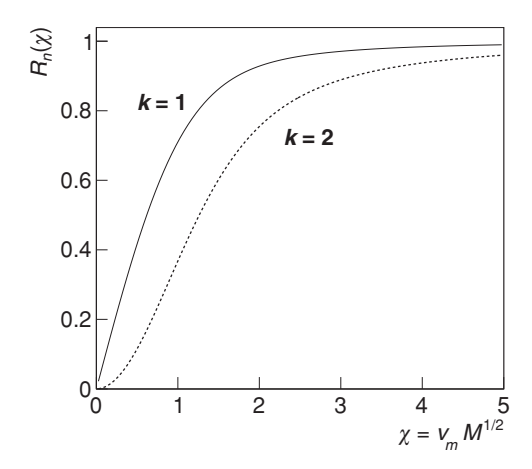


Fig. 11.12

Event plane resolution,  $R_n$ , as a function of  $\chi = v_n \sqrt{M}$ , where  $v_n$  is actual flow, and M is the number of particles involved in the estimation of the event plane resolution. The harmonic number of the correlation n is an integer k times the harmonic number m of the event plane.

the (pseudo)rapidity, charge, or any combination of these criteria. The use of a pseudorapidity gap, in particular, constitutes a straightforward method for suppressing short-range correlations and consequently suppressing nonflow effects.

Three techniques, known as  $\phi$  weighting, recentering, and shifting, are commonly used to correct for detector artifacts in the evaluation of the event plane angle  $\Psi_n$ . They are described in §12.4.4.

## **Two and Multiparticle Correlation Methods**

As discussed in §11.1.2, two-particle densities measured as function of the relative azimuthal angle between two produced particles are sensitive to collective flow. One indeed finds

$$\frac{dN_{\text{pairs}}}{d\Delta\phi} \propto 1 + \sum_{n=1}^{\infty} 2v_n^2 \cos\left(n\Delta\phi\right),\tag{11.131}$$

where all pairs of a particular momentum and rapidity range are selected for the calculation of this pair spectrum. It is therefore possible to obtain the **square** of the flow coefficients,  $v_n$ , from fits of pair azimuthal distributions. This technique is known as the **pairwise correlation method**. Experimentally, this can be readily accomplished by taking measurements of the normalized two-particle density  $r_2(\Delta \phi)$  or the normalized cumulant  $R_2(\Delta \phi)$  since, by construction, these observables yield measurements that are corrected for detection efficiencies. The properly normalized pair spectrum is thus

$$\frac{dN_{\text{pairs}}}{d\Delta\phi} = \frac{\langle n\rangle^2}{\langle n(n-1)\rangle} r_2(\Delta\phi), \tag{11.132}$$

where  $\langle n \rangle$  and  $\langle n(n-1) \rangle$  are the average number of particles and average number of pairs detected in the nominal momentum and rapidity range of the measurement of  $r_2(\Delta \phi)$ ,

respectively. The factor  $\langle n \rangle^2 / \langle n(n-1) \rangle$  is introduced to account for the fact that the numerator of  $r_2(\Delta \phi)$  is proportional to the number of measured pairs while its denominator has an  $n^2$  dependence on the number of particles.

The **two-particle cumulant method** is conceptually identical to the pairwise correlation method. However, instead of carrying out a fit of measured pair spectrum, one evaluates the average of the square of the flow coefficients directly by a measurement of  $\langle \cos[n(\phi_1 - \phi_2)] \rangle$ . Coefficients obtained with this method are denoted

$$v_n\{2\}^2 \equiv \langle \cos[n(\phi_1 - \phi_2)] \rangle, \tag{11.133}$$

where the average is calculated for all (selected) pairs of all (selected) events. It is important to realize that the coefficients  $v_n\{2\}^2$  are actually a measure of the average of the square of the flow coefficient  $\langle v_n^2 \rangle$ . They are thus sensitive to fluctuations as well as the magnitude of the flow coefficients and nonflow effects, as per Eq. (11.112).

It is useful and convenient to introduce the particle unit flow vector  $u_{n,i}$ , defined in the complex plane as

$$u_{n,i} \equiv e^{in\phi_i} = \cos n\phi_i + i\sin n\phi_i, \qquad (11.134)$$

where  $\phi_i$ , as in prior sections, denotes the azimuthal angle of particle *i*. Considering that the number of particles produced below and above the reaction are equal on average, one may write (see Problem 11.10)<sup>3</sup>:

$$\langle u_{n,1}u_{n,2}^*\rangle = \langle \cos n\phi_1 \cos n\phi_2 \rangle = v_2\{2\}^2 \tag{11.135}$$

The unit vector  $u_{n,i}$  consequently provides for an elegant technique to study differential flow (i.e., the flow dependence on transverse momentum and rapidity), known as the **scalar product method**:

$$v_n(p_T, y) = \frac{\langle Q'_{n,i} u^*_{n,i}(p_T, y) \rangle}{2\sqrt{Q^a_n Q^b_n}},$$
(11.136)

where the average  $\langle Q'_{n,i}u^*_{n,i}(p_T,y)\rangle$  is calculated for all particles of interest and averaged over all events. The event plane vector, hereafter expressed in the complex plane, is calculated as

$$Q'_{n,i} = \sum_{j \neq i} w_j u_{n,j}, \tag{11.137}$$

where the coefficients  $w_i$  are weights chosen to optimize the event plane determination. The sum over all particles j excludes particle i in order to avoid autocorrelations. Computationally, one can avoid the recalculation of  $Q'_{n,i}$  for all particles by first computing  $Q_n = \sum_j w_j u_{n,j}$  and using  $Q'_{n,i} = Q_n - u_{n,i}$ . The factor  $2\sqrt{Q_n^a Q_n^b}$ , in the denominator of Eq. (11.136), corrects for the event plane resolution and can be obtained as  $\langle \cos[n(\Psi_a - \Psi_b)] \rangle$ .

<sup>&</sup>lt;sup>3</sup> The product  $u_{n,1}u_{n,2}^*$  yields a term proportional to  $\sin n\phi_1 \sin n\phi_2$ , which is strictly null only in the absence of nonflow correlations.

The scalar method is shown in [10] to yield statistical errors that are slightly smaller than those achieved with the standard event plane method. Indeed, given that the event plane vector  $Q_n$  is in principle based on an arbitrary selection of particles, it can be obtained from single particles. The scalar product then reduces to the event plane method, but with poorer resolution. Additionally, note that division by the event resolution corrects the mean  $v_n$  values obtained but not their statistical fluctuations.

The two-particle correlators defined by Eqs. (11.125,11.133,11.136) are sensitive to collective flow as well as two- and few-particle correlations commonly known as nonflow. They thus tend to overestimate the flow coefficients  $v_n$ . To suppress nonflow contributions, it is thus desirable to utilize correlation functions that are by construction insensitive, or suppress the effects of two-, or few-particle correlations. We saw in §10.2 that cumulants of order n, noted  $C_n$ , are by construction insensitive to correlations of order m < n. Suppression of nonflow, dominated by two-particle correlations, in the determination of flow can thus be accomplished with higher order cumulants. However, note that since the correlators are obtained by averaging over azimuthal angles in the range  $[0, 2\pi[$ , odd order cumulants vanish by construction and are thus of little interest in the context of flow measurements. Measurements of flow, with suppressed nonflow, are thereby achieved with even-order cumulants exclusively. We here restrict our discussion to fourth-order cumulants, but extensions to higher orders are possible and well documented in the literature [182].

The fourth-order cumulant  $C_4$  was first introduced in §10.2.2 in the context of generic particle correlation functions. In the context of azimuthal correlations, it may be written

$$C_4(1, 2, 3, 4) = \rho_4(1, 2, 3, 4) - \sum_{(4)} \rho_1(1)\rho_3(2, 3, 4)$$

$$- \sum_{(3)} \rho_2(1, 2)\rho_2(3, 4) + 2\sum_{(6)} \rho_1(1)\rho_1(2)\rho_2(3, 4)$$

$$- 6\rho_1(1)\rho_1(2)\rho_1(3)\rho_1(4).$$
(11.138)

The indices 1, 2, 3, and 4 are here used as shorthand notations for the azimuthal angle  $\phi_i$ , i = 1, 2, 3, 4, and the sums are carried over terms consisting of permutations of these indices. For flow measurements involving a sum over all 4-tuplets of particles, terms that contain odd-order densities must vanish when calculated for a large event ensemble since the average cosine of unpaired angles vanishes when average over  $[0, 2\pi]$ . The averaged four-cumulant consequently reduces two terms: one involving the four-particle density  $\rho_4(1, 2, 3, 4)$  and the other dependent on the product  $\rho_2(1, 2)\rho_2(3, 4)$ . Here again, it is convenient to use particle flow vectors  $u_{n,i}$  defined in the complex plane. The fourth-order cumulant may thus be written

$$\langle \langle u_{n,1} u_{n,2} u_{n,3}^* u_{n,4}^* \rangle \rangle = \langle u_{n,1} u_{n,2} u_{n,3}^* u_{n,4}^* \rangle - 2 \langle u_{n,1} u_{n,2}^* \rangle \langle u_{n,3} u_{n,4}^* \rangle$$
(11.139)

where the double brackets  $\langle \langle \rangle \rangle$  indicate the correlator is a cumulant. One can verify (see Problem 11.14) that in the absence of flow fluctuations, the four-cumulant is equal to  $-v_n^4$ . One thus defines the fourth-order flow cumulant flow coefficients as

$$v_n\{4\} = \left(-\langle\langle u_{n,1}u_{n,2}u_{n,3}^*u_{n,4}^*\rangle\rangle\right)^{(1/4)}.$$
(11.140)

The  $v_n\{4\}$  notation is universally used to identify flow coefficients determined on the basis of the fourth-order cumulant (11.139). Flow coefficients obtained based on higher order cumulants are likewise noted  $v_n\{6\}$ ,  $v_n\{8\}$ , and so forth. However, note that because higher order cumulants involve the combination (subtraction) of several terms, they may yield negative values resulting from either fluctuations, or limited statistics. Their interpretation may consequently be somewhat challenging, and measurements of these quantities typically require substantially larger data samples to achieve the same statistical significance as that obtained with second-order cumulants.

Cumulants may be determined with generating functions, as discussed in  $\S\S2.13$  and 10.2.2, or by direct calculation.

Other multiparticle cumulants are also of interest in the context of mixed harmonic studies. An important example of such studies involves the measurement of the three-particle correlator

$$\langle u_{n,1}u_{n,2}u_{2n,3}^*\rangle = v_n^2 v_{2n},\tag{11.141}$$

where the particle flow vectors of particles 1 and 2 are calculated at order n while the flow vector of the third particle is obtained at order 2n. This correlator was used successfully at RHIC to suppress nonflow effects in the study of  $v_1$  and  $v_4$  flow coefficients. Mixed harmonics are also extremely useful in studies (searches) of the **chiral magnetic effect** (CME) [125, 124, 183].

## **Q**-Distribution Method

In previous sections, we showed how the event plane vector  $\vec{Q}$  may be used to infer the orientation of the reaction plane of colliding nuclei. But  $\vec{Q}$  also provides information about the magnitude of the flow itself. The flow vector  $\vec{Q}$  may be determined based on a subset of or all measured particles. Its magnitude and direction are thus effectively determined by a random walk process, that which consists of the sum of all particle transverse momentum vectors. In the absence of flow and other forms of particle correlations, the random walk yields a vector  $\vec{Q}$  whose magnitude grows in proportion to the square root of the number of particles M involved in its calculation. But in the presence of flow, that is, for finite flow coefficients,  $v_n$ , the magnitude of the vector grows proportionally to  $Mv_n$ . It is thus convenient to introduce a normalized flow vector

$$\vec{q}_n = \frac{\vec{Q}}{\sqrt{M}} \tag{11.142}$$

whose magnitude should be order unity in the absence of flow, and that should scale proportionally to  $\sqrt{M}v_n$  in the presence of flow. Based on the discussion presented in §2.12.2, we conclude that  $|\vec{q}_n| = v_m \sqrt{M} \langle p_T \rangle$ , where  $\langle p_T \rangle$  is the average transverse momentum of the particles selected for the calculation of  $\vec{Q}$  (corresponding to the average step size in the language of a random walk used in §2.12.2). The magnitude of the flow vector  $\vec{q}_n$  then has the following probability distribution in the large M limit:

$$\frac{1}{N}\frac{dN}{dq_n} = \frac{q_n}{\sigma_n^2} \exp\left(-\frac{v_n^2 M + q^2}{2\sigma_n^2}\right) I_o\left(\frac{q_n v_n \sqrt{M}}{\sigma_n^2}\right). \tag{11.143}$$

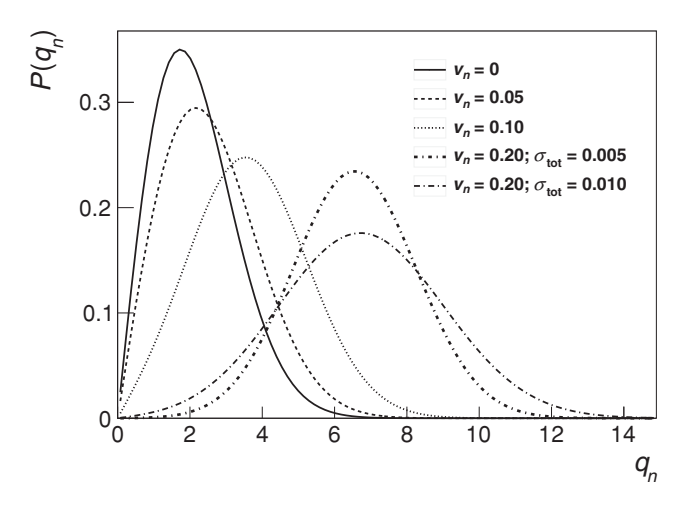


Fig. 11.13 Probability density function of the modulus of the normalized flow vector  $\vec{q_n}$  for selected values of the flow coefficient  $v_n$  and the fluctuation parameter  $\sigma_{\text{tot}}$ .

where  $I_o$  is a modified Bessel function,  $v_n$  are flow coefficients, and  $\sigma_n$  is a measure of fluctuations.

$$\sigma_n^2 = \frac{1}{2} \left( 1 + M \sigma_{\text{tot}}^2 \right),$$
 (11.144)

where

$$\sigma_{\text{tot}}^2 = \delta_n + 2\sigma_{vn}^2 \tag{11.145}$$

As illustrated in Figure 11.13, the presence of flow shifts the distribution toward larger  $q_n$  values, while increased fluctuations, determined by  $\sigma_{\text{tot}}$ , broaden the distribution. The **Q-distribution method** thus consists in estimating  $v_n$  and  $\sigma_n$  based on a fit of a measured  $q_n$  distribution with Eq. (11.143). The method enables the determination of  $\sigma_{\text{tot}}$  but cannot discern the effects of nonflow,  $\delta_n$ , and flow fluctuations  $\sigma_{vn}$  separately.

## Lee—Yang Zeros Method

The Lee-Yang zeros method is based on a technique developed in 1952 by Lee and Yang to detect a liquid-gas phase transition [2, 38, 53]. The technique involves the second-harmonic flow vector  $\vec{Q}_2$  projected onto an arbitrary laboratory direction specified by an angle  $\theta$ :

$$Q_2^{\theta} = \sum_{i=1}^{M} w_i \cos[2(\phi_i - \theta)]. \tag{11.146}$$

The sum is carried out over selected or all particles i with azimuthal angle  $\phi_i$  and weight  $w_i$ . Typically, the projection is evaluated for five arbitrary but equally spaced values of  $\theta$  in order to suppress detector acceptance effects. The method then entails finding the zero(s)

of a complex generating function of the form

$$G_2^{\theta}(ir) = \left| \left\langle e^{irQ_2^{\theta}} \right\rangle \right|, \tag{11.147}$$

where r is variable along the imaginary axis of the complex plane and the average  $\langle \rangle$  is taken over all events of interest. One uses the square of the modulus to determine the location of the first minimum,  $r_a^{\theta}$ , corresponding to an angle  $\theta$ , determined by the integrated flow

$$V_2^{\theta} = j_{01}/r_o^{\theta},\tag{11.148}$$

$$v_2 = \langle V_2^\theta \rangle_\theta / M, \tag{11.149}$$

in which  $j_{01} = 2.405$  is the first root of the Bessel function  $J_0$  and M is the multiplicity of the event. The average  $\langle \rangle_{\theta}$  is taken over the lab angles  $\theta$  and yields the flow coefficient  $v_2$  relative to the reaction plane axis. For implementation details and variants of the method, see, e.g., ref. [182] and references therein.

## Fourier and Bessel Transforms Method

Let  $f_o(Q_{x,n})$  denote the PDF of the x component of the  $Q_n$  flow vector in the absence of flow (i.e.,  $v_n = 0$ ) but finite nonflow correlations. Assume that the presence of a flow field does not otherwise influence the nonflow correlations. By virtue of the central limit theorem, the distribution of  $Q_n$  in the presence of flow can then be obtained simply by shifting the argument of  $f_o$  by an amount that depends on the reaction plane angle  $\Psi$ . Averaging over all values of this angle, one obtains

$$f(Q_{x,n}) \equiv \frac{1}{N} \frac{dN}{dQ_{x,n}} = \int \frac{d\Psi}{2\pi} f_o(Q_{x,n} - v_n M \cos(n\Psi)).$$
 (11.150)

Next calculate the Fourier transform of this function:

$$\tilde{f}(k) = \left\langle e^{ikQ_{n,x}} \right\rangle 
= \int \frac{d\Psi}{2\pi} \int dQ_{x,n} e^{ikQ_{n,x}} f_o(Q_{x,n} - v_n M \cos(n\Psi))$$
(11.151)

Defining  $t = Q_{x,n} - v_n M cos(n\Psi)$ , Eq. (11.151) may then be written

$$\tilde{f}(k) = \int \frac{d\Psi}{2\pi} e^{ikv_n M \cos(n\Psi)} \int dt e^{ikt} f_o(t)$$

$$= J_0(kv_n M) \tilde{f}_o(k),$$
(11.152)

in which one finds that the flow and nonflow contributions to the Fourier transform  $\tilde{f}(k)$  are factorized: the transform  $\tilde{f}_o(k)$  characterizes the nonflow correlations whereas  $J_0(kv_nM)$  expresses the dependence on the flow magnitude  $v_n$ . The zeros of the Fourier transform are determined by the zeros of the Bessel function  $J_0(kv_nM)$ . One may then get an estimate of the flow coefficient  $v_n$  based on the first zero,  $k_1$ , of the Fourier transform

$$v_n = \frac{j_{o1}}{k_1 M} \tag{11.153}$$

where, as in the previous section,  $j_{o1}$  corresponds to the first zero of the Bessel function  $J_0(z)$ , and is equal to  $j_{01} = 2.405$ . This technique, called **Fourier and Bessel transforms method**, is equivalent to the Lee–Yang zeros method covered in the previous section.

A similar reasoning can be applied to the two-dimensional Fourier transform of  $dN/dQ_{n,x}dQ_{n,y}$ . One gets (see Problem 11.15)

$$\tilde{f}(k) = \int dQ_{n,x} e^{ik_x Q_{n,x}} dQ_{n,y} e^{ik_y Q_{n,y}} \frac{d^2N}{dQ_{n,x} dQ_{n,y}}$$

$$= dQ_n J_0(kQ_n) \frac{dN}{dQ_n} \sim J_0(kv_n M).$$
(11.154)

The flow contribution is decoupled from all other correlation contributions. The Bessel transform, Lee–Yang zeros, and *Q*-distribution methods are thus similar if not totally equivalent. See [182] and references therein for a more in-depth discussion of this and related topics.

## 11.4.3 Pros and Cons of the Various Flow Methods

The methods presented in the previous sections may be compared based on their statistical accuracy (for equal data samples) and in their capacity to suppress or disentangle nonflow effects from flow. For instance, two-particle correlations obtained in a relatively narrow pseudorapidity range, with a single harmonic, measures flow in the participant plane, but the use of mixed harmonics, for instance the first harmonic from spectator neutrons and second harmonic for particles produced at central rapidities, should provide elliptic flow in the reaction plane.

Nonflow contributions, noted  $\delta_n$ , are defined by Eq. (11.112) as the excess correlation from two- or few-particle correlations arising from particle production dynamics not related to collective effects (collective behaviors resulting from pressure gradients or differential attenuation determined by the collision geometry) and thus the collectivity of particles produced. Nonflow contributions should therefore be more or less independent of the particles' direction relative to the reaction plane. Sources of nonflow correlations include hadronization in jets, decays of short-lived particles, short-range correlations such as the Hanbury-Brown Twiss (HBT) effect, and energy/momentum conservation. Nonflow correlations tend to be stronger for particles emitted near one another in momentum space, particularly rapidity. It is thus possible to reduce the effects of nonflow in the evaluation of flow coefficients by considering particles emitted in distinct and well separated ranges of rapidity (pseudorapidity) and transverse momentum, or particle pairs with different charge combinations. The scalar product method, in particular, lends itself well to such measurements with a large  $\eta$  gap.

Nonflow effects are dominated by two-, three-, and few-particle correlations. As such,  $\delta_n$  primarily scales as the inverse of the produced multiplicity (see §10.2.3) and thus lead to a nearly constant contribution of  $M\langle u^*\rangle$  on collision centrality while flow's contribution rises and fall from peripheral to central collisions. Note, however, that the contribution of nonflow effects is likely to exhibit a small dependence on collision centrality, in A +A collisions, as a result of the changing relative probability of rare or high- $p_T$  process with

collision impact parameter. Be that as it may, nonflow contributions to the correlator  $\langle uQ^* \rangle$  may be subtracted using the so-called **AA-pp method** given that nonflow contributions to this correlator should be nearly independent of collision centrality. It is worth noting that the AA-pp method can be used for any *n*-particle correlation measurement of harmonic coefficients.

Another technique commonly used to reduce nonflow effects in the determination of flow coefficients is the use of multiparticle cumulants, which by construction suppress by  $\sim 1/M$  for each particle added to a correlator. Indeed, measurements taken at RHIC indicate that four-particle cumulants remove nonflow effects almost completely [182].

An additional uncertainty in the determination of flow coefficients arises from flow fluctuations. For a given collision system, beam energy, and impact parameter, one expects flow to reach an expectation value determined largely by the geometry of the collision system. By the very nature of microscopic systems, fluctuations in the initial geometry or the collision dynamics may occur. One thus expects the flow magnitude to exhibit event-by-event fluctuations. These fluctuations, however, affect the various flow measurement methods quite differently. The effects of flow fluctuations can be expressed formally as follows for two-, four-, and six-particle cumulants:

$$v_n\{2\} = \sqrt{\langle v_n^2 \rangle} = (\langle v_n \rangle^2 + \sigma_v^2)^{1/2}$$
 (11.155)

$$v_n\{4\} = \left(2\langle v_n^2 \rangle^2 - \langle v_n^4 \rangle\right)^{1/4} \tag{11.156}$$

$$v_n\{6\} = \left[ (1/4) \left( \left\langle v_n^6 \right\rangle - 9 \left\langle v_n^4 \right\rangle \left\langle v_n^2 \right\rangle + 12 \left\langle v_n^2 \right\rangle^3 \right) \right]^{1/6}$$
 (11.157)

and so on, for higher-order cumulants. Clearly, while  $v\{2\}$  is directly sensitive to  $\langle v \rangle$  and  $\sigma_v$ , higher cumulants require knowledge of higher order moments of the distribution in v. Models can, however, be invoked to estimate the relations between these moments. For instance, in the limit of a Gaussian flow distribution, one finds [185]

$$v_n\{2\} = \left(\langle v_n \rangle^2 + \sigma_v^2 \right)^{1/2} \approx \langle v_n \rangle + \sigma_v^2 / (2\langle v \rangle) \tag{11.158}$$

$$v_n\{4\} = \left(\langle v_n \rangle^4 - 2\sigma_v^2 \langle v_n \rangle^2 - \sigma_v^4\right)^{1/4} \approx \langle v_n \rangle - \sigma_v^2 / (2\langle v \rangle)$$
(11.159)

$$v_n\{6\} = \left(\langle v_n \rangle^6 - 3\sigma_v^2 \langle v_n \rangle^4\right)^{1/6} \approx \langle v_n \rangle - \sigma_v^2 / (2\langle v_n \rangle) \tag{11.160}$$

We thus conclude that while flow fluctuations increase the magnitude of the coefficients estimated from two-particle correlations ( $v\{2\}$ ), they reduce by an approximately equal amount the values obtained with four- and six-particle cumulants. The preceding relations strictly hold only if  $\sigma_v \ll \langle v \rangle$ . However, the flow vector distribution is, as we saw in §11.4.2, not perfectly Gaussian. Including effects of flow fluctuations, one gets [185]:

$$\frac{1}{N} \frac{dN}{v_n dv_n} = \frac{1}{\sigma_n^2} \exp\left(-\frac{v_n^2 + v_{n,o}^2}{2\sigma_n^2}\right) I_o\left(\frac{v_n v_{n,o}}{\sigma_n^2}\right). \tag{11.161}$$

where  $v_{n,o}$  is the nominal value of the flow coefficient (i.e., its expectation value,  $v_{n,o} = \langle v_n \rangle$ ). The  $v_2$  cumulants can then be shown to be

$$v_2\{2\} = v_{2,o}^2 + 2\sigma_v^2, (11.162)$$

$$v_2\{n\} = v_{2,n} \text{ for } n \ge 4.$$
 (11.163)

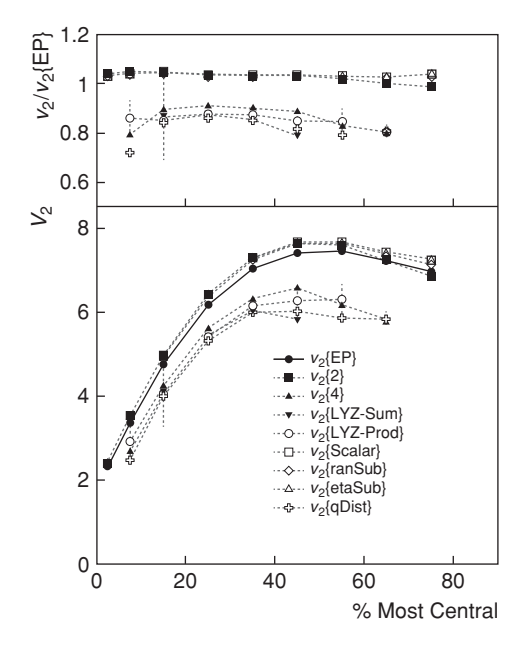


Fig. 11.14

Ratio of the elliptical flow coefficients  $v_2$  obtained by several methods to those obtained with the event plane method in the analysis of charged hadrons measured in Au + Au collisions at  $\sqrt{s_{NN}} = 200$  GeV [2, 7]. Ratios are shown for the random subevents, pseudorapidity subevents, scalar product, two-particle cumulants, four-particle cumulants, Q-distribution, and Lee-Yang zeros sum generating and product generating functions. (Data from STAR collaboration [182].)

Effects of nonflow on the event plane method are more complicated to evaluate but have been shown to range from  $v_2\{EP\} = v_2\{2\} = \langle v^2 \rangle^{1/2}$  to  $v_2\{EP\} = \langle v \rangle$ , depending on the reaction plane resolution [19]. The dependence of fluctuations of the Lee-Yang zeros method and its derivatives are nonlinear [184]. For Bessel-Gaussian distributions in v, these methods yield the same results as higher cumulants, namely  $\langle v \rangle = v_o$  of the Bessel-Gaussian distribution. Consequently, if the  $v_2$  distribution is Bessel-Gaussian, all multiparticle methods should yield the same result:  $\langle v \rangle = v_o = v_{2,RP}$  [37].

To summarize, we note that the event plane method is a special case with results ranging between  $v_2\{2\}$  and  $v_2\{4\}$  depending on the reaction plane resolution. Higher-order cumulants  $v_2\{6\}$  and Lee-Yang zeros results, however, tend to agree quantitatively with  $v_2\{4\}$ , as illustrated in Figure 11.14.

# 11.5 Appendix 1: Numerical Techniques Used in the Study of Correlation Functions

The calculation of products, such as  $\rho_1 \otimes \rho_1(\Delta \phi)$  and  $\rho_1 \otimes \rho_1 \otimes \rho_1(\Delta \phi_{12}, \Delta \phi_{12})$  required in the measurements of two-particle cumulant  $C_2(\Delta \phi)$  and three-particle cumulant

 $C_2(\Delta\phi_{12}, \Delta\phi_{12})$ , is in principle based on integrals over coordinates  $\phi_1$ ,  $\phi_2$ , and  $\phi_3$  (see, e.g., Eq. (11.10)). In practice, the densities  $\rho_1(\phi_i)$  are estimated on the basis of histograms with a finite number of bins. One must thus replace the integrals over continuous variables by sums running over the histograms bins:

$$\rho_{1}\rho_{1}(\Delta\phi_{12}) \equiv \rho_{1}\rho_{1}(m) \tag{11.164}$$

$$= \sum_{i,j=1}^{n} \rho_{1}(i)\rho_{1}(j)\delta_{m,j-i}$$

$$\rho_{1}\rho_{1}\rho_{1}(\Delta\phi_{12}, \Delta\phi_{13}) \equiv \rho_{1}\rho_{1}\rho_{1}(m, p)$$

$$= \sum_{i,j,k=1}^{n} \rho_{1}(i)\rho_{1}(j)\rho_{1}(k)\delta_{m,j-i}\delta_{p,k-i}.$$

The indices i, j, k are used to specify the  $\phi$  bins of particles 1, 2, and 3, respectively, while the integer variables m and p correspond to bins in  $\Delta\phi_{12}$  and  $\Delta\phi_{13}$ , respectively. The delta functions ensure the proper match between  $\Delta\phi_{ij}$  and the difference  $\phi_i - \phi_j$ . This procedure assumes a one-to-one bin mapping. With  $n_{\phi}$  bins in  $\phi$  for each particle, this would require twice as many bins for the angle difference. However, given the periodicity of the  $\phi$  and  $\Delta\phi$  variable, one may transform the integers m and p according to

if 
$$m = i - j < 0$$
 then, replace  $m$  by  $m + n_{\phi}$ . (11.165)

and similarly for p. The number of bins in  $\Delta \phi$ , is consequently  $n_{\Delta \phi} = n_{\phi}$ . The aforementioned technique may similarly be applied to the determination of the terms  $\rho_2 \otimes \rho_1(\Delta \phi_{ij}, \Delta \phi_{ik})$  of the  $C_3$  cumulant. One gets

$$\rho_{2}\rho_{1}(m,p)_{123} = \sum_{i,j,k=1}^{n} \rho_{2}(i_{1},j_{2})\rho_{1}(k_{3})\delta_{m,i_{1}+j_{2}}\delta_{p,i_{1}+k_{3}}$$

$$\rho_{2}\rho_{1}(m,p)_{231} = \sum_{i,j,k=1}^{n} \rho_{2}(i_{2},j_{3})\rho_{1}(k_{1})\delta_{m,i_{1}+j_{2}}\delta_{p,i_{1}+k_{3}}$$

$$\rho_{2}\rho_{1}(m,p)_{132} = \sum_{i,j,k=1}^{n} \rho_{2}(i_{1},j_{2})\rho_{1}(k_{3})\delta_{m,i_{1}+j_{2}}\delta_{p,i_{1}+k_{3}},$$
(11.166)

where the indices  $i_l$ ,  $j_l$ , and  $j_l$  refer to bins in  $\phi$  for particles l and the variables m and p correspond to bins in  $\Delta \phi_{ij}$  and  $\Delta \phi_{ik}$ , respectively, as specified by the delta functions, and meant to satisfy the periodic boundary condition expressed by Eq. (11.165).

The aforementioned numerical technique is defined for finite width bins in  $\phi$  and  $\Delta\phi$ . This implies a given bin in  $\Delta\phi$  spans a range wider than its nominal width  $2\pi/n_{\Delta\phi}$ . For instance, for i=j=0 one has  $\phi_i$  and  $\phi_j$  span the range  $2\pi/n_{\phi}$ . The difference  $\phi_i-\phi_j$  consequently spans the range  $[-2\pi/n_{\phi}, 2\pi/n_{\phi}]$  which is obviously wider than  $[0, 2\pi/n_{\Delta\phi}]$  for  $n_{\Delta\phi}=n_{\phi}$ . The signal from a specific  $\Delta\phi$  bin is thus effectively smeared across three bins in the numerical integrations of Eqs. (11.164) and (11.166). This effect, commonly known as **bin aliasing**, cannot be avoided but may be suppressed by use of a rebinning technique: first, calculate the integrals with  $n_{\Delta\phi}=n_{\phi}$ , and subsequently rebin the integrated signals to

575 Exercises

have  $n_{\Delta\phi}/m$  bins using m as an integer multiple of 2. A value of  $m\gg 2$  will greatly reduce the effects of the bin sharing. However, this may demand a large amount of statistics if the rebinning is applied on  $R_2$  or  $R_3$  to account for instrumental or detection inefficiencies.

The integration techniques expressed in Eqs. (11.164) and (11.166) can readily be applied to studies of correlations in  $\Delta \eta$  rather than  $\Delta \phi$ . However, note that since no periodic boundary can be assumed in  $\Delta \eta$ , one must map the differences  $\eta_1 - \eta_2$  obtained from  $n_{\eta}$  bins onto  $n_{\Delta \eta} = 2n_{\eta} - 1$  bins in  $\Delta \eta$ . This leads to the mapping

$$m = i - j$$
 replaced by  $m + n_{\Delta n} + 1$ , (11.167)

$$\rho_1 \otimes \rho_1(m) = \frac{1}{H_m(m)} \sum_{i,j=1}^n \rho_1(i)\rho_1(j)\delta(m-i+j+n_{\Delta\eta}+1)$$
 (11.168)

and with similar expressions for  $\rho_1 \otimes \rho_1 \otimes \rho_1(m, p)$  or  $\rho_2 \otimes \rho_1(m, p)$  (see Problem 11.9).

## **Exercises**

- **11.1** Verify that the difference  $\nu \nu_{\text{stat}}$  yields Eq. (11.69).
- **11.2** Verify the scaling property expressed by Eq. (11.76).
- **11.3** Verify the scaling property expressed by Eq. (11.77).
- **11.4** Show that the quantity  $\omega_Q$  defined by Eq. (11.78) tends to unity in the independent particle production limit.
- **11.5** Derive the equations (11.80) for the charge conservation limit in elementary or nuclear collisions that produce particles over a range of rapidity spanning several units.
- **11.6** Find an expression similar to Eq. (11.91) for the event-wise average  $\langle p_T \rangle$  defined by Eq. (11.89). Hint: Express  $\rho_1(\eta, \phi, p_T)$  as a sum of conditional cross sections  $\rho_1(\eta, \phi, p_T|m)$ , defined for a fixed event multiplicity m and each with probability P(m), i.e.  $\rho_1(\eta, \phi, p_T) = \sum_m P(m)\rho_1(\eta, \phi, p_T|m)$ .
- **11.7** Find an expression similar to Eq. (11.97) for the event-wise average  $\langle \Delta p_T \Delta p_T \rangle$  defined by Eq. (11.93). Hint: Decompose  $\rho_2(\eta_1, \phi_1, p_{T,1}, \eta_2, \phi_2, p_{T,2})$  as a sum of conditional cross sections  $\rho_2(\eta_1, \phi_1, p_{T,1}, \eta_2, \phi_2, p_{T,2}|m)$  similar to the decomposition of  $\rho_1(\eta, \phi, p_T)$  used in Problem 11.6.

**11.8** Show that the correlation  $\langle \Delta p_T \Delta p_T \rangle_I^{(m)}$  applied to a colliding consisting of a superposition of m independent but identical processes, each with covariance  $\langle \Delta p_T \Delta p_T \rangle_I^{(1)}$ , scales as

$$\langle \Delta p_T \Delta p_T \rangle_I^{(m)} = \frac{1}{m} \langle \Delta p_T \Delta p_T \rangle_I^{(1)}. \tag{11.169}$$

- **11.9** Find expressions equivalent to Eq. (11.168) for the averages  $\rho_1 \otimes \rho_1 \otimes \rho_$
- **11.10** Verify that the product  $\langle u_{n,1}u_{n,2}^*\rangle$  averaged over an ensemble events has a vanishing contribution from sine terms  $\sin n\phi_1 \sin n\phi_2$ .
- **11.11** Define a "triggered" correlation function  $K_T(\Delta \phi)$  in terms of a two-particle cumulant  $C_2$ .
- 11.12 One expects the strength of the  $\nu_{+-,\rm dyn}$  correlation function to be largely determined by the charge production mechanism. For instance, the production and decay of neutral resonances, such as the  $\rho$ -meson, should have a large impact on net charge fluctuation measured values of  $\nu_{+-,\rm dyn}$ . This can be illustrated with a simple model that includes the production of three particle types,  $\pi^+$ ,  $\pi^-$ , and  $\rho^o$ . Assume the three species are produced independently and with relative fractions  $p_1$ ,  $p_2$ , and  $p_3$  respectively. Ignore effects associated with Bose statistics and assume the probability of producing  $n_1$   $\pi^+$ ,  $n_2$   $\pi^-$ , and  $n_3$   $\rho^o$  may be expressed with a multinomial distribution:

$$P(n_1, n_2, n_3; N) = \frac{N!}{n_1! n_2! n_3!} p_1^{n_1} p_2^{n_2} p_3^{n_3}.$$
 (11.170)

Further assume that all  $\rho^o$ s decay into a pair  $\pi^+$  and  $\pi^-$  and calculate the magnitude of dynamic fluctuations  $\nu_{+-,dyn}$ .

- **11.13** Verify that Eq. (11.50) is correct in cases where  $\langle N_+ \rangle = \langle N_- \rangle$ .
- **11.14** Verify Eq. (11.139) and show that the fourth-order cumulant equals  $-v_n^4$  in the absence of flow fluctuations.
- **11.15** Demonstrate Eq. (11.154).